CHALMERS
UNIVERSITY OF TECHNOLOGY

Fluid Structure Interaction and Non-Newtonian Blood Flow in Stent Grafts for Abdominal Aortic Aneurysms

Master's thesis in Applied Mechanics

AMITH BALASUBRAMANYA

Department of Applied Mechanics
CHALMERS UNIVERSITY OF TECHNOLOGY
Gothenburg, Sweden 2016

Master's thesis 2016:75

Fluid Structure Interaction and Non Newtonian Blood Flow in Stent Grafts

Amith Balasubramanya

CHALMERS
UNIVERSITY OF TECHNOLOGY

Department of Applied Mechanics
Division of Fluid Dynamics
Chalmers University of Technology
Gothenburg, Sweden 2016

Typeset in LaTeX
Gothenburg, Sweden 2016

FSI and non-Newtonian blood flow in stent grafts for AAA
Amith Balasubramanya
Department of Applied Mechanics
Chalmers University of Technology

Abstract

Abdominal aortic aneurysm(AAA) is a common problem encountered which leads to dilation of the abdominal aorta. One novel way of treating AAA is using endovascular aortic repair (EVAR) where a polymer stent graft (SG) is used to redirect blood flow. Post operative concerns are common with EVAR like stent graft migration that are caused due to displacement forces acting on the ends of the SG. In this thesis, the aim is to correlate experimental results with a developed computational model which is used to evaluate forces acting on the ends of an iliac limb stent graft. Chosen liquid for the experiment was water as pressure is said to be the main driving force and viscous effects are negligible. Displacement forces are numerically evaluated using a finite volume approach for fluid-structure interaction (FSI) with the open source tool OpenFOAM for different pressures (145/80, 170/90, 195/100 mm.Hg) and different stroke rates (60, 80 and 100 BPM). Further, different blood viscosity models are studied and a comparison of forces for Newtonian and non-Newtonian blood models are presented. Wall shear stress(WSS) and velocity contours are presented for both blood models and complex flow phenomenon like secondary flow structures are explained. Viscous forces are found to be negligible and pressure is the main cause of displacement forces which is consistent with the experiment and justifies the usage of water in the experiment. Newtonian and non-Newtonian models yielded similar results for displacement forces as that of water and small variations were observed in velocities and WSS.

Keywords: AAA, Stent graft, FSI

Acknowledgements

I would like to take this opportunity to thank the division of fluid dynamics, Chalmers university of technology for its warm and ambient atmosphere which was integral to carry out this work. This work wouldn't have been possible without my supervisors, Hakan Nilsson for his unending patience, belief in my skill and timely discussions and Srdjan Sasic for his infectious enthusiasm and eye openers regarding non-Newtonian flows during the course of this work. Special thanks to Hakan Roos at Sahlgrenska hospital for always helping me out with questions regarding physiology and a medical standpoint. Special mention to Anirudh Rao, for his unwavering support and his patience to answer even the smallest of questions, life in academia and perspectives on things, technical and well as personal. My friends at the department, Abhishek, Raju, Srikanth who have always been there to help me out and fruitful, lively discussions at odd hours about topics a plenty. This wouldn't have been possible with the support of my parents, especially my father who has been a pillar not only during the course of this thesis, but my entire masters program.

Amith Balasubramanya, Gothenburg,October,2016

Contents

1 Introduction **1**
- 1.1 Background . . . 1
- 1.2 Purpose . . . 1
- 1.3 Literature survey . . . 2
  - 1.3.1 Displacement forces and stent graft migration . . . 2
  - 1.3.2 Non-Newtonian flow . . . 3
  - 1.3.3 Secondary flow structures . . . 3
- 1.4 Assumptions and limitations . . . 3

2 Theory **5**
- 2.1 Mathematical Formulation of Fluid Equations . . . 5
- 2.2 Mathematical Formulation of Solid Equations . . . 5
- 2.3 Fluid Structure Interaction . . . 6
- 2.4 Viscosity Models . . . 7
- 2.5 Similarilty Parameters . . . 8
  - 2.5.1 Reynolds Number . . . 8
  - 2.5.2 Womersley number . . . 8
  - 2.5.3 Dean Number . . . 9
- 2.6 Experimental Setup . . . 9
- 2.7 Physiological Input . . . 11

3 Methodology **13**
- 3.1 Geometry and Mesh . . . 13
- 3.2 Material Properties . . . 14
- 3.3 Boundary Conditions . . . 15

4 Results **17**
- 4.1 Viscosity Models . . . 17
- 4.2 Forces and Displacement . . . 18
  - 4.2.1 Water . . . 18
  - 4.2.2 Blood . . . 19
- 4.3 Flow structures . . . 22
  - 4.3.1 Peak velocity (t)=0.1 s . . . 23
  - 4.3.2 Peak deceleration at (t)=0.4 s . . . 24
  - 4.3.3 End of deceleration at (t)=0.6 s . . . 25
  - 4.3.4 End of diastole at (t)=0.85 s . . . 26

4.3.5 Wall shear stress (WSS) 27

5 Conclusion and Future Work **33**

5.1 Observations and Conclusions 33

5.2 Future Work 33

1

Introduction

In this thesis, 3D Fluid structure interaction(FSI) analysis is perfomed for a stent graft. Preliminary analysis is conducted with water to evaluate forces that lead to migration of the stent graft and it is validated with the existing experimental results by Roos et al[16]. Further, analysis is performed with blood as the fluid medium to study wall shear stresses and evaluate non-Newtonian effects. Even though the non-Newtonian effects may not have a significant effect on the displacement forces, it is interesting to see the difference in flow structures formed by assuming blood as Newtonian and subsequently a non-Newtonian fluid.

1.1 Background

Abdominal Aortic Aneurysm (AAA) is irreversible dilation of the abdominal aorta that occurs commonly among males over the age of 65[11] .Common surgical procedures include insertion of a stent graft which is a wire mesh woven around a synthetic and flexible graft material [13] to redirect flow of blood in the diseased artery. Two most commonly preferred surgical methods are open aortic repair (OAR) and endovascular aortic repair (EVAR). OAR involves stitching the stent graft with the blood vessel [16] and in EVAR, a graft is inserted from iliac limbs to the affected area such that the aneurysm isn't affected by the pulsatile blood flow. EVAR can lead to post operative complications like endoleaks which is blood flow into the cavity surrounding the stent graft, graft migration and eventually rupture. Stent graft migration is of utmost importance when there is distal(downstream) movement in the proximal(upstream) portion of the stent graft.

Experimental work was performed evaluating the displacement forces that cause stent graft migration by Roos et al[16], but water was chosen as the fluid medium. A computational model was setup by Anderson and Pilquist[2] which is considered as a baseline but realistic boundary conditions were not considered. Other computational studies have been performed that estimate the magnitude of forces and the biomechanical factors that lead to migration [11, 13].

1.2 Purpose

The aim of this thesis is to computationally validate the experiments conducted by Roos et al[16]. In the paper, they attributed the use of water instead of blood stating that the shear component of forces contribute 1 to 3 % of the total displacement forces and hence the viscous effects would be negligible. Hence, the contribution of viscous forces needs to be studied. Pressure is said to be the major contribution for displacement forces and this needs to be shown during the course of the thesis. Subsequently, blood is used as the fluid medium and displacement forces are calculated to show that the results for blood and water are similar. Blood is a non-Newtonian fluid, hence different viscosity models for blood are studied to understand its true nature. Even though, viscosity isn't a major contribution to the developed forces, understanding the secondary flow structures developed due to local geometry effects and comparing Newtonian and non-Newtonian flows might provide an insight into flow structure and vortex formation in stent grafts.

1.3 Literature survey

The overall perspectives on the thesis can be summarized as displacement forces, blood viscosity, flow in stent grafts and an attempt to explain the complex secondary flow structures formed. Literature on each of these are studies separately to give better insight.

1.3.1 Displacement forces and stent graft migration

Important work on flow in stent grafts, their displacement forces and stent graft migration was performed in a series of papers by Li and Kleinstruerer[13, 12, 11]. In [13], FSI studies were performed for a diseased aneurysm and results were compared with a stented aneurysm. After placement of stent graft, noticeable changes were observed in the surrounding pressure, maximum wall stress. Geometric parameter changes also affect the developed drag force. Pressure in the surrounding regions, maximum wall stress significantly decreased. It was also observed that increase in exit pressure boundary conditions significantly increased drag forces. According to [12], stagnant blood around the stent graft will turn into an intraluminal thrombi(ILT) that applies additional pressure on the outer-wall of the graft. This pressure affects the drag force or displacement forces acting on the stent graft. In [11], the drag force curve obtained behaves similarly as pressure. Increase in diameter of the stent graft shows a larger drag force developed. Also, the paper states that the contribution of viscous forces is 1% to % where pressure is said to be the main driving component.
According to [1], increase in iliac limb angulations i.e. increase in bend of the pipe increases sideways displacement forces and contributed to 91 % of the total displacement forces. Liffman et al [14] suggested that when self expanding forces are used in stent grafts, the downward forces may exceed the force required to dislodge the graft. However, when the angulation increases, sideways component increases which adds additional force to dislodge the graft and eventually lead to migration. The paper also produced analytical solutions with and without gravity which could be useful in cases where patient specific geometry is not utilized, such as ours. However, the three papers mentioned here do not utilize fluid structure interactions and assume the graft material to be rigid.
To sum it up, increase in diameter, exit pressure and graft angle increases the drag

force (displacement force). Also, drag force behaves similar to the exit pressure waveform. Also, viscous contribution is 1 to 3% of the total displacement forces.

1.3.2 Non-Newtonian flow

Flow in large arteries usually assume that blood flow is usually Newtonian but this is not the case always. Li and Kleinstreurer utilized the Quemada non-Newtonian viscosity models (which is an extension of the Casson model discussed in 2.4). Specific studies where Newtonian and non-Newtonian model contributions to displacement forces are far from few. One such study where FSI with non-Newtonian fluids on a stent graft is performed by Janela et al[8]. They observed that a non-Newtonian model have a very small impact on graft sideways displacement comapred to the Newtonian model. Most studies utlize a Carreau non-Newtonian model to model blood while studying displacement force components [14, 5]. Work by Figueroa et al and Curien et al utilize a Newtonian model and see no observable differences in the magnitude of displacement forces[1, 6]
Extensive studies have been done where Newtonian and non-Newtonian models have been compared [9, 10]. These studies are however for the entire aorta. We can however assume similar flow structures formed when there are no angulations in the graft. There are observable changes in the peak velocity and flow structures developed during the entire cardiac cycle between the models. To conclude, most studies utilize non-Newtonian models while simulating arterial flows, however for stent grafts, studies are far from few comparing different models. More studies specific to non-Newtonian regimes and viscosity models are in section 2.4

1.3.3 Secondary flow structures

According to [20], secondary flows are developed when there is centripetal acceleration that causes a radial pressure gradient to be developed. This pressure gradient drives the slower moving fluid near the vessel wall towards the center, while the faster moving fluid at the core is moved outwards. These are very common in physiological flows. According to [20], these flows are governed using Dean's number (D_e) which occurs in curved structures. Hence, larger the Dean number, larger the acceleration. Ishikawa[7] performed a study using the Bingham non-Newtonian model and noted that the non-Newtonian effects tend to weaken the strength of the vortex and are more prevalent during Low Reynolds' numbers. Malony et al stated that taper towards the distal end reduces velocity magnitude and eventually the secondary flow structures formed. Biasetti et al [3] studied the vortex structures formed using the lambda 2 method over the cardiac cycle in a patient specific aneurysm.

1.4 Assumptions and limitations

- Blood is considered a single phase fluid in this work and the compressibility effects are neglected. Blood in reality, is a multiphase fluid in which, the red blood cells and leukocytes are chosen as the dispersed phase and surrounding plasma is chosen as the carrier phase. Due to already existing complexity in the problem statement, multiphase nature of blood is not modelled.

- Majority of flows that are physiological in nature especially in large arteries are laminar. Onset of turbulence is unclear in these kind of flows according to literature. Hence, the effects of turbulence on the flow structures are not considered.
- A stent graft consists of a flexible graft material on which a wired mesh stent is woven. The stent however is geometrically and numerically difficult to model and hence only the graft material is modeled. The graft material is assumed to be linear, isotropic material so the anisotropic effects of the solid material are not considered.
- According to Li and Kleinstruerer[12], increase in sac pressure (pressure applied by stagnant blood on the stent graft wall) after EVAR might be a cause of stent graft migration. However, sac pressure is not taken into account.
- Only half section of the graft is modelled to save computational time. This could pose as a problem due to the fact that the developed flow structures may not be symmetrical.
- The effect of gravity is not considered i.e. the patient is assumed to lying horizontally
- Only one distal extension of the iliac limb is modelled.

2
Theory

A finite volume(FV) approach is utilized to discretize the fluid and solid governing equations. Section 2.1 gives an overview of the governing equations for fluid medium using the Eulerian formulation. Section 2.2 gives an overview of the solid governing equations using the updated Lagrangian formulation. Section 2.3 explains the coupling algorithm for fluid and solid equations in the solver. Section 2.4 explains the different viscosity models, their merits and limitations. Section 2.5 lists the dimensionless numbers used that help determine dynamic similarities between the model setup and physical stent graft. Section 2.6 gives a brief overview of the experiments by Roos et al[16]. Finally, section 2.7 shows how signal analysis is performed and final velocity profiles are obtained to be utlized for simulation.

2.1 Mathematical Formulation of Fluid Equations

The fluid equations are solved using the Eulerian approach. Solution of the flow field is calculated using the PISO (pressure implicit with splitting of operator) algorithm, which is an iterative procedure for solving equations for velocity and pressure whilst solving transient problems. First an initial guess of the pressure and velocity fields are made using discretized equations of momentum and then corrected using a discretized pressure correction equation. The only noticeable change is in the momentum conservation equation where the effect of gravity is ignored (assume that the patient is lying still) and hence the term with body force vanishes. Final form of the momentum equation for fluids is given as:

$$\frac{\partial u}{\partial t} = -\nabla p + \mu \cdot (\nabla^2 \cdot u) \tag{2.1}$$

2.2 Mathematical Formulation of Solid Equations

Solid equations are solved using the updated Lagrangian formulation. Displacements and motion of the structural part are obtained which is in-turn transferred to the fluid equations. If we consider a continuum with a Volume, V_s and bound by a Surface, S_s, the governing fluid equations are given by

$$\frac{d}{dt}\int_{V_s} \rho dV_s + \oint_{S_s} n_s.\rho(v - v_s s)dS = 0 \tag{2.2}$$

which gives the conservation of mass and

$$\frac{d}{dt}\int_{V_s}\rho v dV_s + \oint_{S_s} n_s.\rho(v - v_s s)v dS_s = \oint_{S_s} n_s.\sigma dS_s + \int_{V_s}\rho f_b dV_s \tag{2.3}$$

which gives the conservation of momentum. Final form of linear momentum updated in a Lagrangian formulation is given by

$$\int_{V_s}\rho_s\frac{\partial\delta v}{\partial t}dV_s - \oint_{s} n_s.(2\mu+\lambda)\nabla\delta u dS_s = \oint_{S_s} n_s.q dS_s + \int_{V_s}\rho_s\delta f_b dV_s \tag{2.4}$$

where q is given as

$$q = \mu(\nabla u)^T + \lambda tr(\delta u)I - (\mu+\lambda)\nabla\delta u + \mu\nabla\delta u.(\delta u)^T + \frac{1}{2}\lambda(\nabla\delta u : \nabla\delta u)I + \sum_s .\delta F_s \tag{2.5}$$

where q is the tensor that consists of nonlinear as well as coupling terms.The complete derivation of the final form of the solid governing equations and also the discretization procedure is given by Jasak and Tukovic[19]. It is interesting to note that a finite volume formulation is utilized to discretize the solid equations. Typically a mixed finite volume-finite element method is utilized to solve FSI problems[2]. There are advantages and limitations using a finite volume approach to discretize the solid equations. the advantage being there is a single node between solid and fluid interface which doesn't lead to sudden gradients being formed. Also, leakage of the fluid domain into the solid domain as observed by Anderson and Pilquist [2] isn't noticeable in this approach. Disadvantages of this approach is the fact that the solid domain needs to have appreciable thickness and this approach wouldn't be applicable to thin or shell geometries as they would have negligible thickness.

2.3 Fluid Structure Interaction

Coupling of fluid and solid governing equations is an integral process. The system of equations for fluid and solid domains are solved separately and sequentially for each time step. Flow field calculation is performed as mentioned in 2.1. Shear and pressure forces are obtained after each time step once the solution of the flow field is converged and are assembled into a traction vector. The traction is then introduced into the structural equations in the final form as shown in 2.5 and as seen in figure 2.1a. Structural displacements are obtained by solving the system of discretized linear momentum conservation equations for an elastic solid in the updated Lagrangian description as shown in 2.2. Finally, the fluid and structural meshes are both moved in accordance with the calculated displacements and this procedure is iterated till the displacement residual reaches the specified convergence criteria. The steps of the solution procedure can be summarized as seen in figure

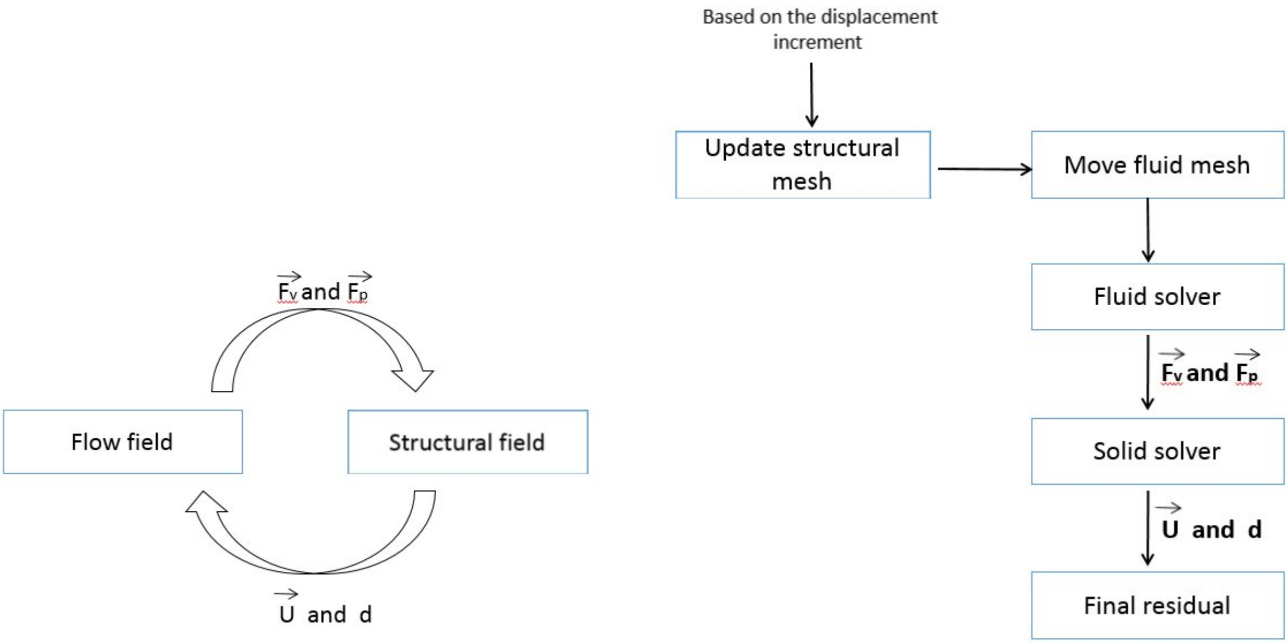

Figure 2.1: Coupling algorithm explained as (a) shows the transfer of forces from flow field to the structral field and (b) shows flow chart after coupling takes place.

2.4 Viscosity Models

Viscosity of blood is an important hemodynamic parameter as it helps compute wall shear stresses, which is an indicator of many diseases. Comprehensive work on compiling different blood viscosity models is done by Yilmaz and Gundogu [21]. As explained by [9], there is no one universally accepted non-Newtonian blood model as strain rates vary from 1 to 1000 s^{-1} over a cardiac cycle. In large arteries, blood is usually assumed to be Newtonian. However, Johnston et al and Karimi et al[9, 10] stated that Newtonian behaviour is valid when the strain rate exceeds $100s^{-1}$ and is a common occurrence in large arteries. So at lower shear rates, blood behaviour is strictly non-Newtonian. Non-Newtonian behaviour can be further categorized as shear thinning, thixotropy and viscoelasticity. Thixotropy and viscoelasticity are transient in nature and are said to be of secondary importance as they vanish at exceeding strain rates[15]. Hence, shear thinning is the widely accepted blood non-Newtonian behaviour. Blood viscosity models as seen in table 2.1 are mathematical formulations obtained using parameter fitting experimental data . Experimental works regarding blood viscosity have been widley conducted by Cho et al and Skalak[4, 17]. The models shown in table 2.1 are the ones available within the solver. There are many more viscosity models for blood , however we restrict ourself to the ones shown in the table.

Casson model is the most widely utilized blood model, but tends to predict higher viscosity near Newtonian conditions. It takes into account Hematocrit(H) which is

Viscosity Model	Effective Viscosity
Casson	$\mu(\dot{\gamma}) = \sqrt{\mu_c} + \sqrt{\frac{\tau_c}{\dot{\gamma}}}$;$\mu_c = 0.00414$,$\tau_c = 0.0038$
Carreau	$\mu(\dot{\gamma}) = \mu_\infty + (\mu_o - \mu_\infty)[1 + (\lambda\dot{\gamma})^2]^{\frac{n-1}{2}}$ $\mu_o = 0.056Pa - s$,$\mu_\infty = 0.0035Pa - s, \lambda = 3.313005, n = 0.3568$
Cross	$\mu_{\dot{\gamma}} = \mu_\infty + \frac{(\mu_o - \mu_\infty)}{1+(\lambda\dot{\gamma})^a}$; $\mu_o = 0.0364Pa - s, \mu_\infty = 0.0035Pa - s, \lambda = 0.38, a = 1.45$
Herschel Bulkley	$\mu_{\dot{\gamma}} = k(\dot{\gamma}) + \frac{\tau_y}{\dot{\gamma}}$
Power Law	$\mu_{\dot{\gamma}} = k(\dot{\gamma})^(n - 1); k = 0.017, n = 0.708$

Table 2.1: Viscosity relations for different non-Newtonian models

the concentration of red blood cells (RBC's). Carreau model fits the experimental set of data provided by [4] and since it's a bounded model, computational cost significantly reduces [3]. As observed from the table, when shear rates tend to zero Casson, Cross and Herschel-Bulkley tend to infinity, hence they aren't bounded. Cross model is an extension of Carreau model which can also be used to simulate blood. This model has been used by [10], but over-predicted the non-Newtonian effectiveness. Power law model works well for mid shear ranges and has a linear behaviour. It over predicts the non-Newtonian behaviour at higher shear rates.

2.5 Similarilty Parameters

While modelling physiological flows, a geometrical similar definition is a natural starting point. However, dynamic similarity needs to achieved as well which means that the modelled system must reach the real flow dynamics. This is achieved through similarity parameters.

2.5.1 Reynolds Number

The Reynolds number(R_e) for an internal pipe of diameter(d) is given by

$$R_e = \frac{\rho U d}{\mu}$$

Physically, the Reynolds number can be described as the ratio of inertial forces to the viscous forces. It can also be represented as the ratio between Momentum flux and wall shear stress. However, it must be noted that μ is the Newtonian viscosity and for non-Newtonian fluids R_e varies as a function of shear stress and strain rates. R_e helps in determining regions where the intertial effects are more dominant than the viscous effects and vice-versa. This is particularly useful in our current setup.

2.5.2 Womersley number

The Womersley number(α)is used for unsteady flows especially pulsatile flows that are common in the human body. α can be represented mathematically by

$$\alpha = \frac{d}{2}\sqrt{\frac{2\pi}{\nu T}}$$

The physical significance can be explained as ratio between diameter and the laminar boundary layer growth over time period T.

2.5.3 Dean Number

In curved planar geometries, secondary flow structure formation is a common phenomenon. This can be evaluated using Dean Number D_e. It is givenby the formula

$$D_e = 4\sqrt{\frac{D}{r}}R_e$$

Physically it can be represented as balance between inertial force, viscous forces and centripetal forces. Hence, radius of curvature (r) and Reynolds number (R_e) affect D_e. D_e plays a major role in determining local curvature effects.

2.6 Experimental Setup

An experimental setup to resemble aortic perfusion is constructed where, water at room temperature is forced in a circuit consisting of a roller pump and silicone tubing . Roller pump is used to simulate a heart beat and peripheral resistance is achieved with water/air-filled container in combination with pinch valves. By adjusting the pinch valves and water level in the containers, the fluid pressure could be altered with high accuracy. To minimize disturbances in the pulse curve, an additional water/air container is used to dampen the velocities. Obtained beats at the inlet is converted to velocity and used as a boundary condition.
An iliac limb stent graft (135 X 16 mm) was inserted into the circuit and fixed at its proximal and distal ends to a strain gauge load cells as shown in 2.2. Values are measured for different angulations and stroke frequencies of the stent graft. One major assumption is that the fluid chosen is water as the density of water and blood like fluids are of similar magnitudes and viscosity of the fluid does not play a major role in determining the outcome of the forces developed. Also, the measurement of pressure is delayed at the outlet by a small duration. This time lag is not considered in the outlet boundary condition and the measurement is considered instantaneous in the computational model.

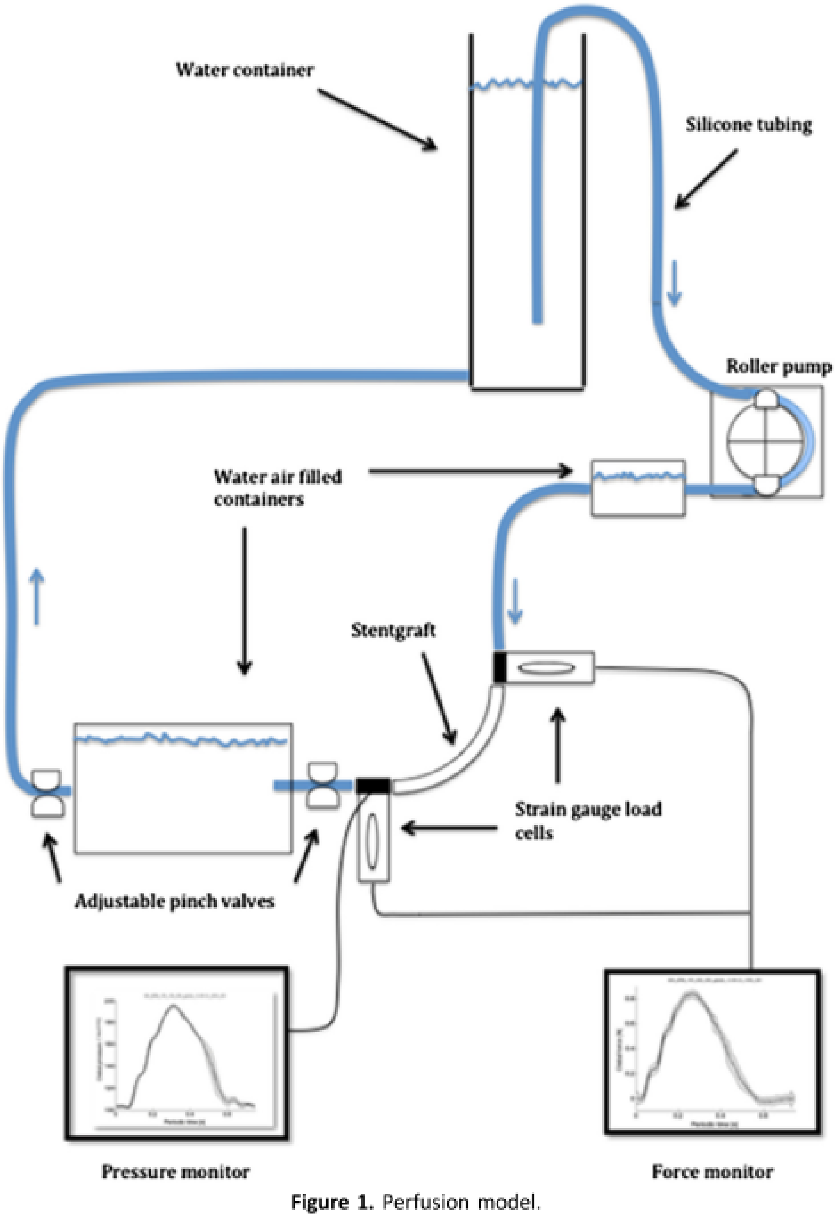

Figure 2.2: Experimental Setup (Figure reproduced with permission from Håkan Roos[16]

2.7 Physiological Input

The experimental data received is in the form of beats per minute as shown in figure 2.3. This data is converted to velocity by assuming an ideal stroke volume ($mL/beat$). Experimental flow rate for different stroke frequencies can be found in Roos et al[16]. Final velocity is achieved and signal analysis is carried out by ensemble averaging the obtained velocities. Hence the final achieved pressure and velocity are averaged over 9 seconds of time to give 1 second of pulse. Final velocity is calculated using the formula

$$\left\langle U \right\rangle = \lim_{N\to\infty} \frac{1}{N} \sum_{n=1}^{N} U_n$$

Note that the averaging time may vary depending on the trial in the experiment, hence an averaged value of 5 experimental trials are taken as the final value.

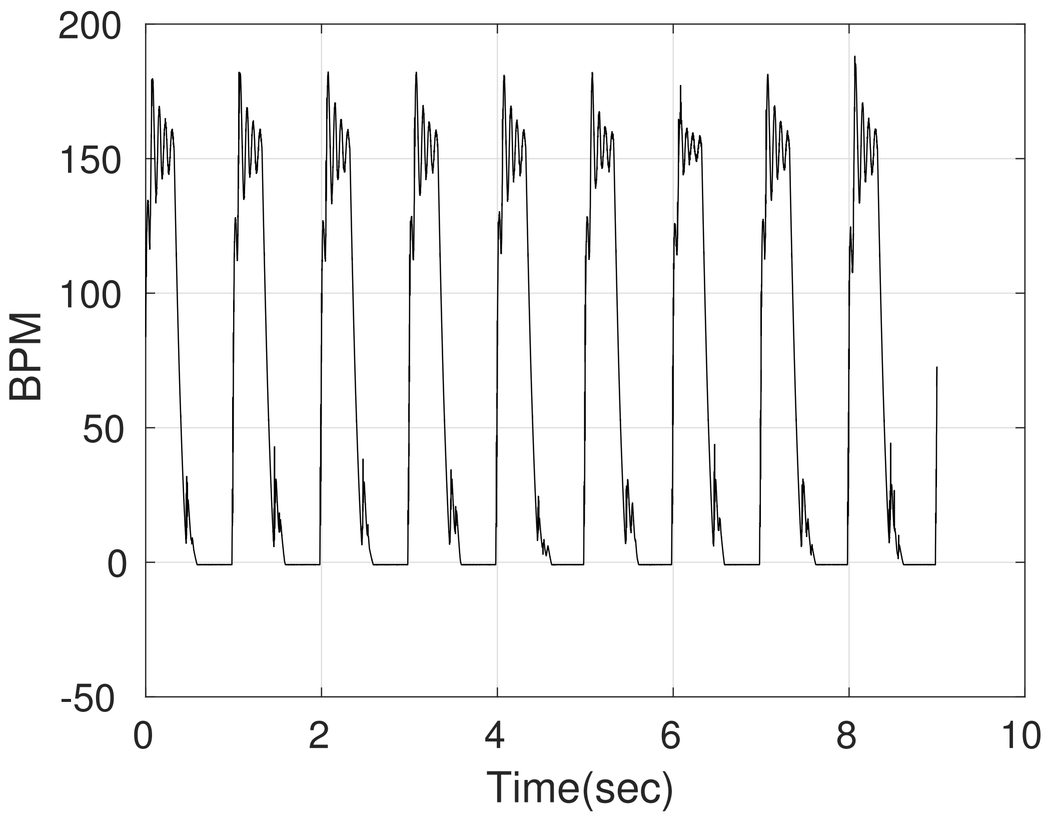

Figure 2.3: Physiological BPM data measured from the experiment for 60 BPM, 145/80 mm.Hg

3
Methodology

This chapter explains the computational setup to obtain numerical values of forces ad displacement. Section 3.1 shows the geometry and mesh that are utilized for the simulation. Section 3.2 lists the material properties for the fluid(blood) and solid(e-PTFE). Finally, section 3.3 shows the boundary conditions used to solve the set of governing equations.

3.1 Geometry and Mesh

The geometry can be chosen as a flexible pipe, but the entrance and exit region are chosen as rigid as seen in figure 3.1. The entrance length (L_e) is chosen as $L/2$ [2], however an accurate value of L_e is tough to determine in our case as the L_e of non-Newtonian fluids can vary from $3D$ to $9D$ [9], where D is the characteristic length of the domain.

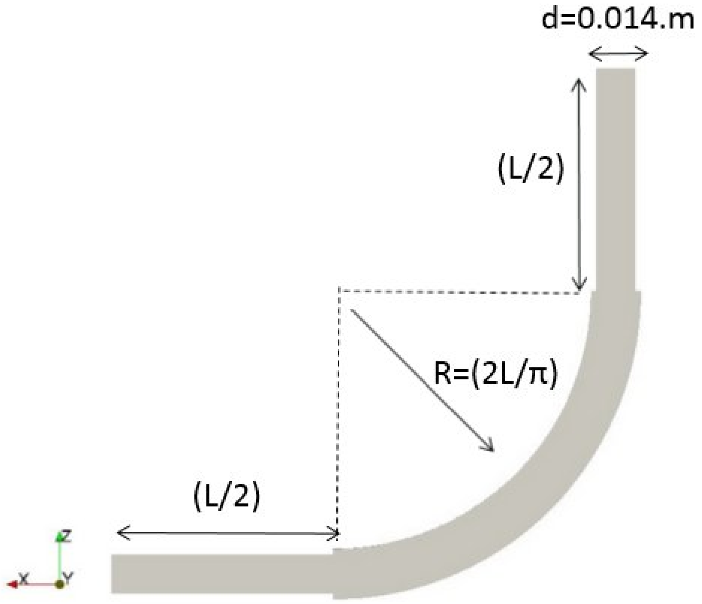

Figure 3.1: Geometrical setup of the case

Figure 3.2 explores the meshes used during simulation and 3.2a shows the blocking structure. Figure 3.2b highlights meshing in the flexible region, where the dark blue region highlights the structural mesh and lighter inner region highlights the fluid region. A separate fluid and solid mesh is generated and merged together using the meshing platform ICEM CFD. $108,360$ hexagonal elements are used.

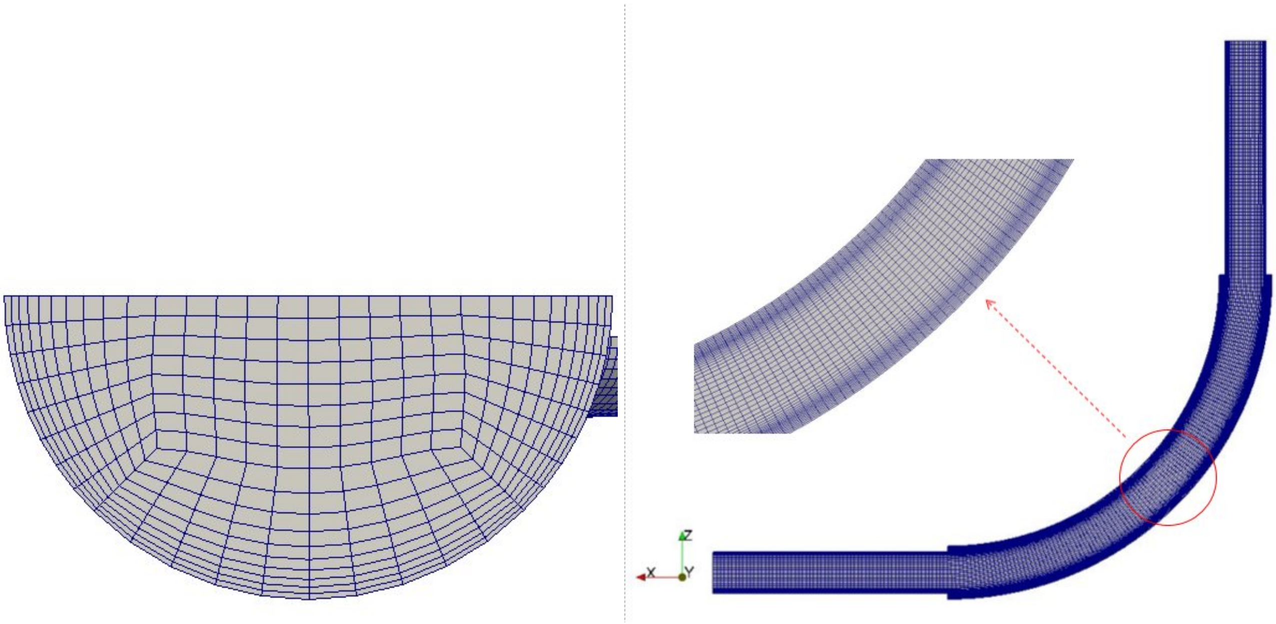

Figure 3.2: Fihure showing (a)Front view of the mesh and (b) Mesh of the whole geometry and highlighting mesh in the flexible region

3.2 Material Properties

The stent graft used is a Gore Excluder iliac limb stent graft(135 x 16 mm) which has e-PTFE flexible graft material and Nitinol stent material. Since, we are not taking into account the stent, the material properties of the graft are as follows. Non-linear effects of the graft material are not considered and a linear elastic model is considered for solid

Graft properties

- Thickness of the graft= 2.mm
- Young's Modulus(E)= 1. Mpa
- Poisson's ratio = 0.27

Fluid properties

- Density (ρ)= 1060 $\frac{kg}{m^3}$ for blood and 1000 $\frac{kg}{m^3}$ for water

- Blood viscosity Newtonian is taken as $\mu = 0.0035 Pa - S$
- Blood viscosity non-Newtonian is given by the Bird-Carreau viscosity model as $\mu = \mu_0 - \mu_\infty[1 + (\lambda\gamma)^2]^{\frac{n-1}{2}}$ where $\mu_0 = 0.056 Pa - s$, $\mu_\infty = 0.0345 Pa - s$, $n = 0.3568$, $\lambda = 3.313 s$

3.3 Boundary Conditions

Inlet velocity profile as shown in ref is used and outlet pressure as shown in 3.3 is used. It is important to note that the curves generated in figure 3.3b are only for 60

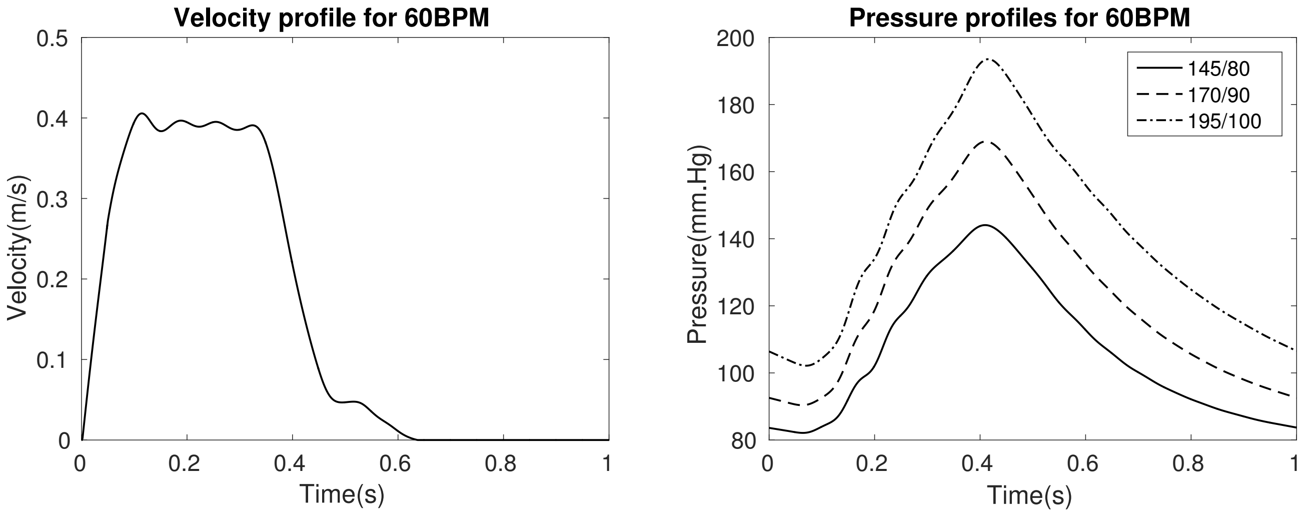

Figure 3.3: Profiles showing (a) Inlet velocity and (b) Outlet pressure boundary conditions

BPM. Similar profiles are genrated for different stroke frequencies and simulations are conducted for all.

Table 3.1 shows the common boundary conditions used to solve the setup of system of governing equations. A zero displacement boundary condition is used for the solid domain which means only after the first time step will there be a motion and coupling as discussed in section 2.3. Velocity and pressure profiles change for each stroke frequency and perfusion pressure.

Boundary	**Type of condition**
Inlet	Input as seen in figure 3.3a
Outlet	Output as seen in figure 3.3b
Rigid wall	No-slip
Fixed wall	Moving wall velocity
Symmetry	Symmetry plane

Table 3.1: Tabular column showing boundary conditions used in the simulation

4

Results

This chapter explains results obtained after performing numerical simulations based on setup discusseds in Chaper 3. Section 4.1 gives a brief perspective on choice of viscosity model suitable for this problem statement.Section 4.2 provides an insight on correlation of numerical results with the experiment and reasons why they maybe different and also forces obtained by Newtonian and non-Newtonian blood models. Section 4.3 and 4.3.5 provide insights on flow structures developed, their complex nature and behaviour of wall shear stress across the geometry and the its impact.

4.1 Viscosity Models

Determining which non-Newtonian model to utilize for blood is a difficult choice owing its complex nature. Here, we try to understand how blood behaves in a channel flow of width D and length $30D$. The section chosen is long enough for the flow to be fully developed. This is a preliminary study in trying to understand which viscosity model for blood to use from the existing ones implemented in the solver. Blood behaves like a Newtonian fluid at shear rates greater than 100 s^{-1} [10, 21]. Keeping that in mind, Carreau, Cross and Casson viscosity models show that behaviour in figure 4.1. However, the Carreau model shows a better correspondence to previously tested blood viscosity by [17]. It shows a good correspondence in the non-Newtonian regime compared to Casson which is important from the perspective of current work being carried out. Power-Law follows a linear behaviour as expected. Herschel-Bulkley shows good correspondence in the non-Newtonian regime however, it tends to a Newtonian behaviour at a higher strain rate than desirable. Hence, out of the existing viscosity models implemented in the solver, the Carreau model is utilized to simulate non-Newtonian blood flow. Also, the bounded nature of Carreau models help in faster computation times compared to non-linear blood viscosity models.[3] which was also discussed in section 2.4

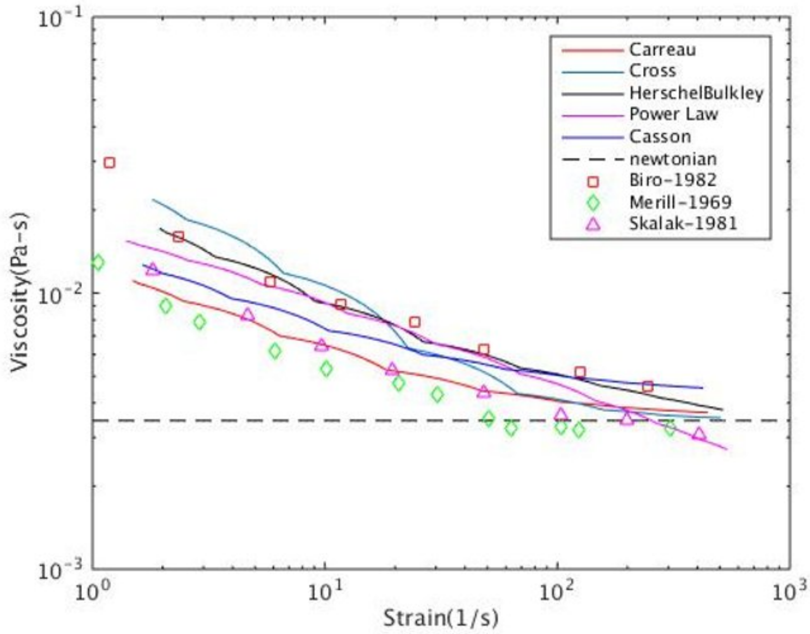

Figure 4.1: Viscosity Profiles for a 2D pipe far upstream

4.2 Forces and Displacement

4.2.1 Water

Water is chosen as the fluid medium initially. This is done to check the efficacy of the developed computational model and also to validate the obtained results with Roos et al [16]. Inlet velocity is shown as specified in the figure 4.9a and outlet pressure as per 4.9b.
Computationally obtained results are shown in plots 4.2, 4.3 and 4.4. We observe that the displacement forces increase with rise in stroke frequency and perfusion pressure which is consistent with literature. Experimentally obtained values according to Roos et al[16] are shown in table 4.1. The gradient of variation between the experiments and numerically obtained forces are similar except for 195/100 mm.Hg. For 195/100 mm.Hg, the forces seem to be of a similar magnitude compared to the experiments.
Since the computational model is quasi-symmetrical in nature, the total displacement force acting is calculated using

$$F = \sqrt{(F_{proximal})^2 + (F_{distal})^2}$$

[16] and for a peak pressure of 195/100 mm.Hg and 100 BPM, it is $2.4621.N$ and similar to computational result obtained by [11] and experiments by [16].
The exact reason for variation from the experiment is difficult to point out but it could be attributed to the assumptions both in the experimental and well as the numerical model. The transience in the plot could be attributed to the discretization scheme used for gradient terms.

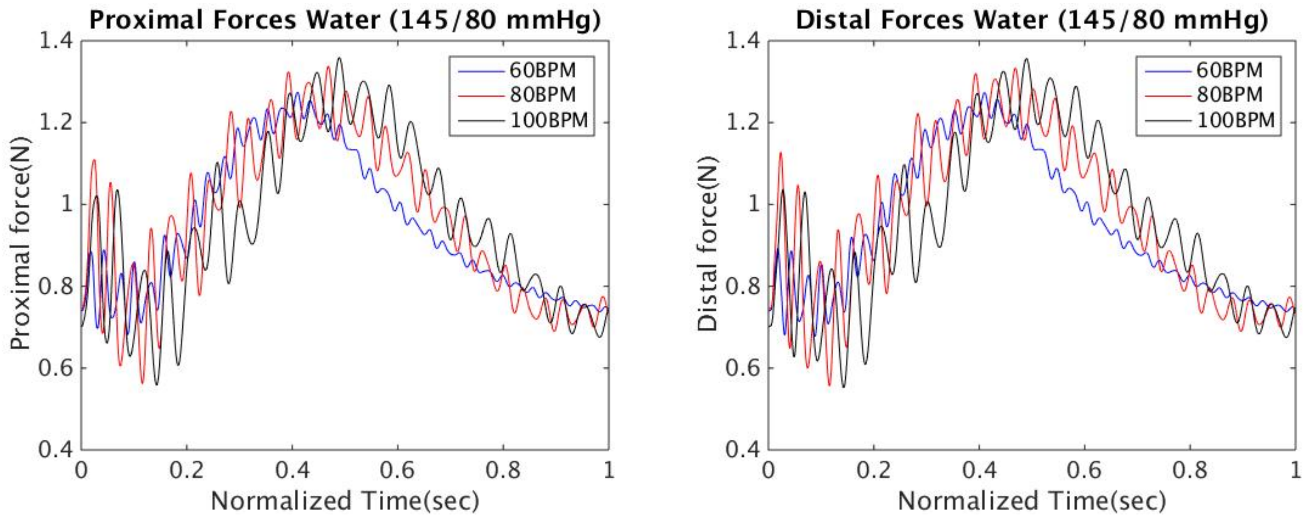

(a) **(b)**

Figure 4.2: Displacement forces (a)Upstream and (b)Downstream for water at 145/80 mmHg and different stroke frequencies

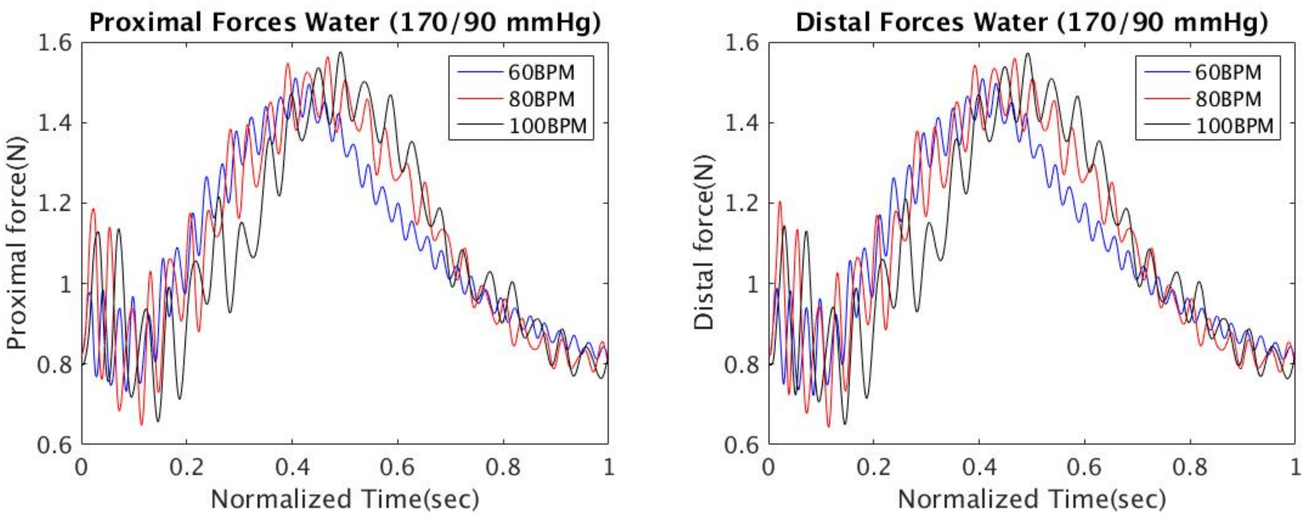

(a) **(b)**

Figure 4.3: Displacement forces (a)Upstream and (b)Downstream for water at 170/90 mm.Hg and different stroke frequencies

4.2.2 Blood

Blood is subsequently chosen as the fluid medium for the same boundary conditions as section 4.2.1. Simulations are performed choosing a constant Newtonian blood viscosity and a non-Newtonian Bird-Carreau viscosity model. The results are compared for each stroke frequency and exit pressure waveform. As observed from

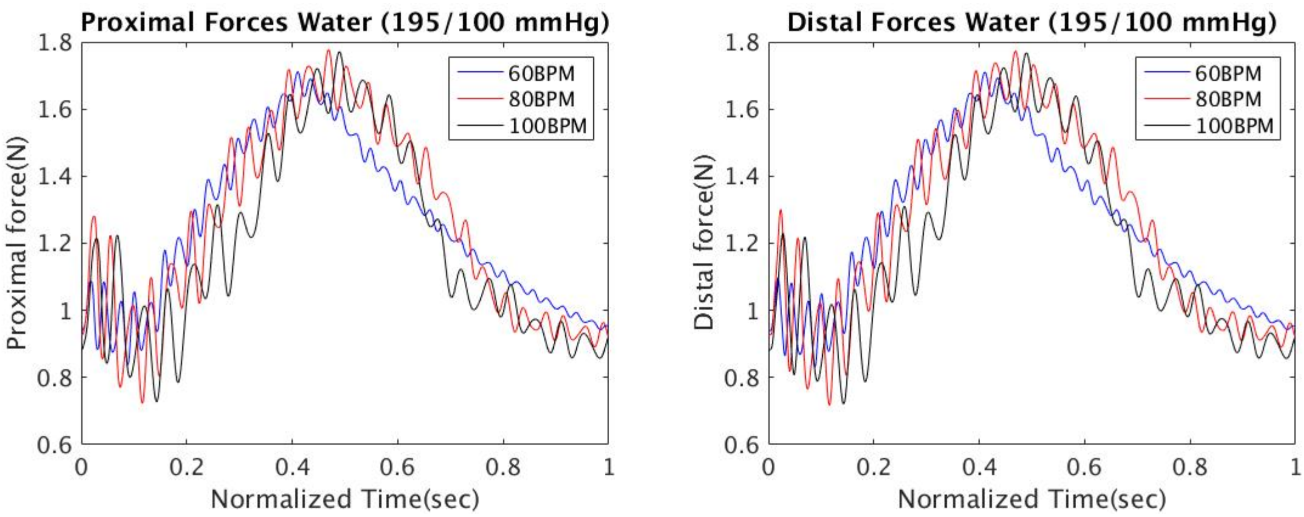

(a) **(b)**

Figure 4.4: Displacement forces for water at 195/100 mm.Hg and different stroke frequencies

Stroke Frequency	Pressure (mmHg)	Experimental Forces(N)		FSI forces water(N)		FSI forces Newtonian blood (N)		FSI forces non-Newtonian blood (N)	
		Proximal (N)	Distal (N)	Proximal (N)	Distal (N)	Proximal (N)	Distal (N)	Proximal (N)	Distal (N)
60BPM	145/80	0.85±0.07	0.92 ±0.03	1.274	1.273	1.264	1.263	1.264	1.263
	170/90	1.28 ±0.04	1.36 ±0.01	1.510	1.508	1.482	1.482	1.481	1.481
	195/100	1.69±0.03	1.78±0.02	1.710	1.710	1.691	1.693	1.689	1.692
80BPM	145/80	0.85 ±0.02	0.86 ±0.03	1.337	1.333	1.332	1.329	1.331	1.326
	170/90	1.28±0.05	1.32±0.05	1.563	1.559	1.559	1.555	1.558	1.552
	195/100	1.70 ±0.07	1.76±0.06	1.776	1.772	1.767	1.764	1.766	1.760
100BPM	145/80	1.01±0.12	1.02±0.08	1.358	1.356	1.339	1.337	1.337	1.333
	170/90	1.35±0.07	1.39±0.03	1.576	1.573	1.558	1.555	1.556	1.551
	195/100	1.71±0.05	1.77±0.03	1.770	1.767	1.746	1.743	1.743	1.739

Table 4.1: Table comparing experimentally and numerically obtained displacement forces for different pressure waveforms and stroke frequencies

figures 4.5,4.6 and 4.7, the behaviour is similar to that of water. With increase in stroke frequencies and perfusion pressure, the magnitude of displacement forces increase. It is interesting to note that the magnitude of displacement forces are the same for water and blood as seen in table 4.1. This could be attributed to the fact that the viscous forces play a very minor role in contribution to the displacement forces[11, 16].

It is also observed that Newtonian and non-Newtonian displacement forces are of similar magnitude. But, forces aren't an accurate comparison of Newtonian and non-Newtonian comparison. As seen in figure 4.8, the contribution of viscosity to the final displacement force is negligible where pressure plays the major role and also the comparison of forces between Newtonian and non-Newtonian show an insignificant variation of viscous forces.

An interesting observation comparing results from section 4.2.1 and the current sec-

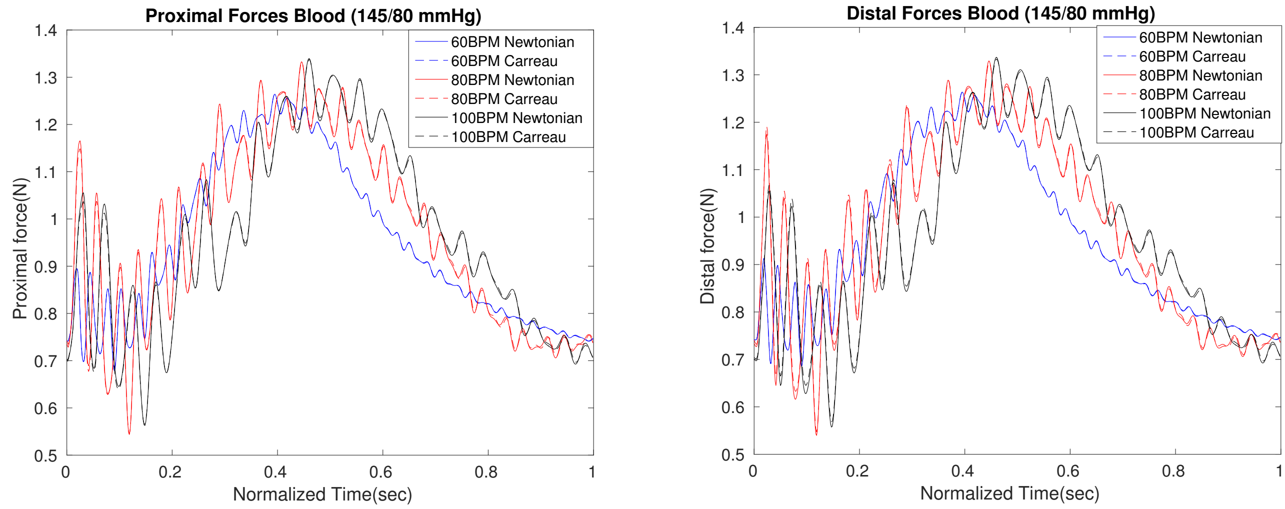

(a) **(b)**

Figure 4.5: Displacement forces for Newtonian and non-Newtonian blood models (a) Upstream and (b)Downstream at 145/80 mm.Hg and different stroke frequencies

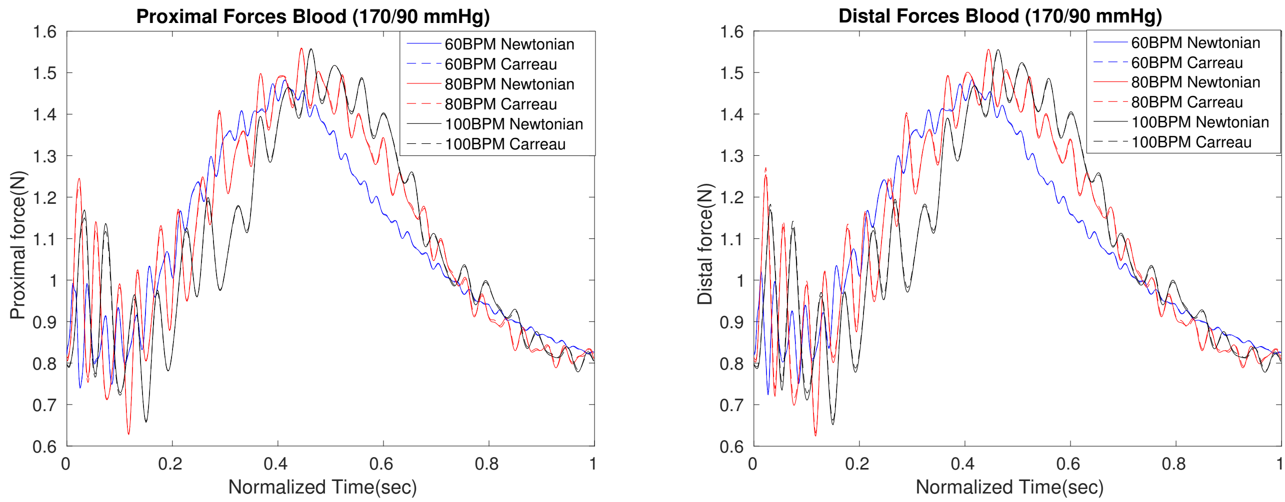

(a) **(b)**

Figure 4.6: Displacement forces for Newtonian and non-Newtonian blood models (a)Upstream and (b)Downstream at 170/90 mm.Hg and different stroke frequencies

tion is that the two fluids are slightly out of phase. These could be attributed to the varying Womersley number. However, further analysis on this needs to be done to check response of Newtonian and non-Newtonian models with different phases in the cardiac cycle similar to work done by [10].

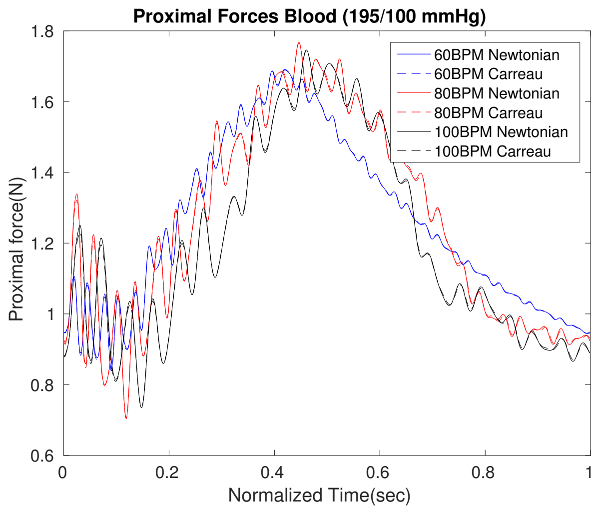

(a)

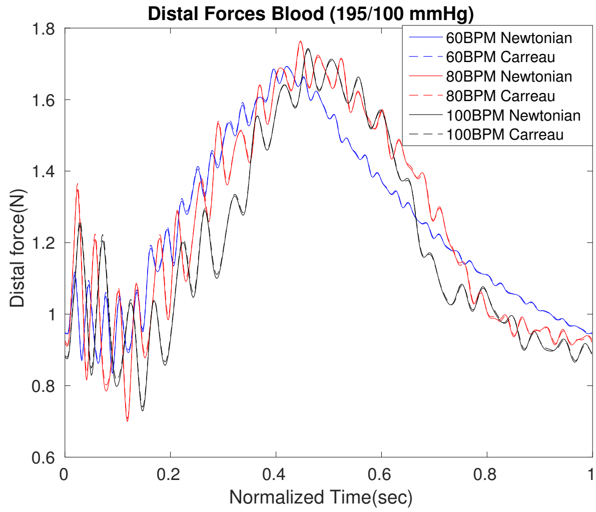

(b)

Figure 4.7: Displacement forces for Newtonian and non-Newtonian blood models (a)Upstream and (b)Downstream at 195/100 mm.Hg and different stroke frequencies

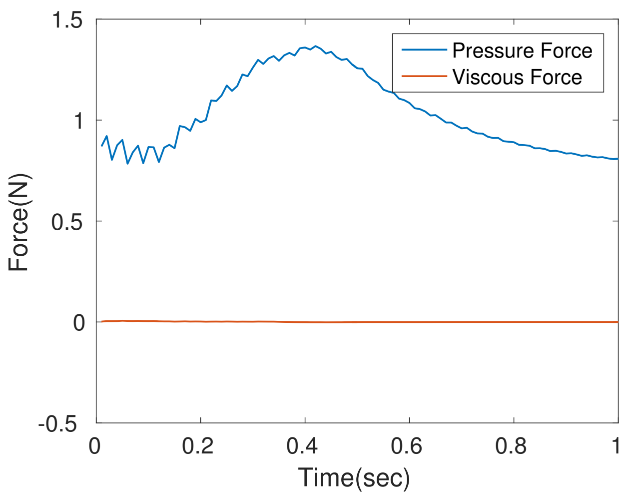

(a) Comparing pressure and viscous forces

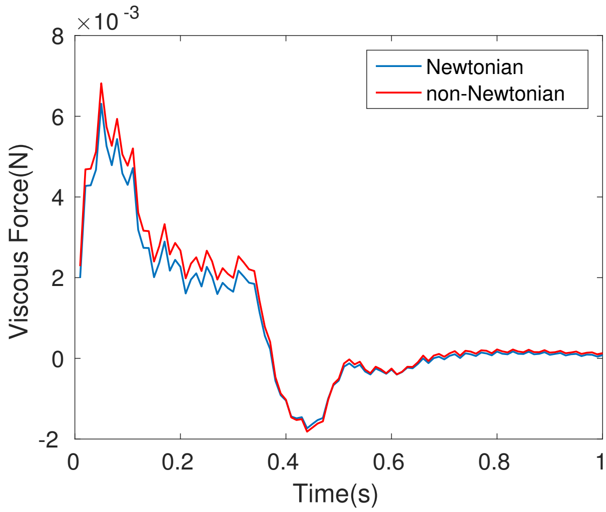

(b) Viscous forces for Newtonian vs non-Newtonian

Figure 4.8: For a 145/80 mmHg and 60BPM case (a) Comparison of pressure and viscous force and (b) Comparison between Newtonian and non-Newtonian blood viscosity models, are shown

4.3 Flow structures

This section gives an insight into the flow structures developed inside the stent graft. These flow structures are usually complex in nature but we will attempt to explain them in order to compare the different viscosity models. It must be kept in mind that smallest scales of turbulence are not considered and a symmetry condition is

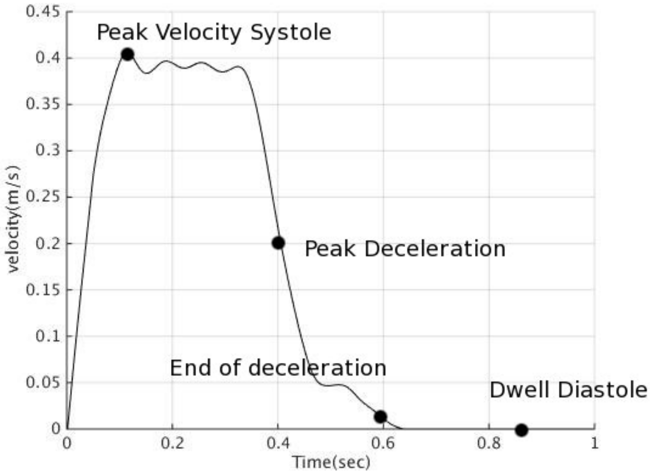

(a) Inlet velocity waveform

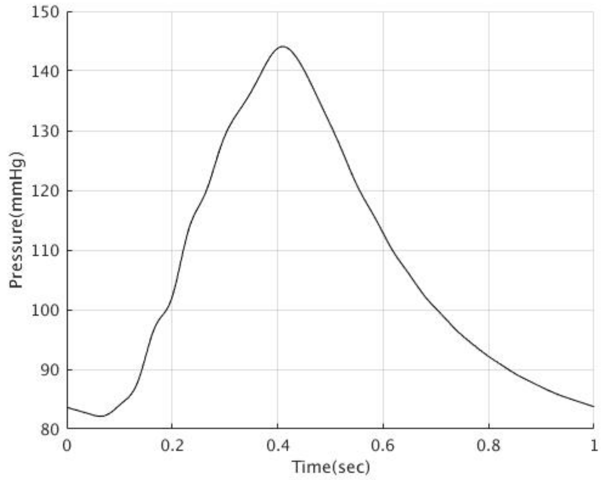

(b) Exit pressure waveform

Figure 4.9: Inlet and Outlet waveforms for 60BPM, 145/80 mm.Hg

assumed. As discussed in 1.4, the flow structures developed may not be symmetrical hence, the velocity contours obtained may not give an accurate description of flows in such geometries. As the entrance and the exit region of the fluid region are considered rigid ,sudden onset of coupling (between fluid and solid) may generate transience, hence the results are calculated after one complete cardiac cycle.
Inlet velocity is given by 4.9a and outlet pressure is given by 4.9b. Flow is evaluated at four intervals which are thought to be of importance. At time(t)=0.1 seconds where peak velocity is obtained. At t = 0.4 seconds where peak deceleration is observed. At t = 0.6 seconds where the deceleration is complete and the diastolic period starts and at t = 0.85 seconds where viscous effects might be observed.

4.3.1 Peak velocity (t)=0.1 s

At t = 0.1 seconds, the inertial effect dominates and as seen from 4.14, no significant difference between the velocity magnitudes for Newtonian and non-Newtonian model. As explained in 3.1, entrance length (L_e) needs to be varied as the calculation of the same depends on R_e and this changes depending on the model. Hence, the flow entering the flexible region need not fully developed as observed in plot 4.10a at the entrance and the exit as seen in plot 4.11a. However, the magnitude of velocities between the two models vary slightly. Far downstream effects on the rigid section maybe attributed to effects from the previous cycle and hence can be neglected at this instant of time. Velocity contours upstream are seen in figures 4.12a, 4.12e for Newtonian and non-Newtonian respectively. We observe upstream that the non-Newtonian plug region is larger. This could indicate a more developed flow compared to Newtonian model. We however find a more uniform distribution downstream with small variations as seen in 4.13a and 4.13e

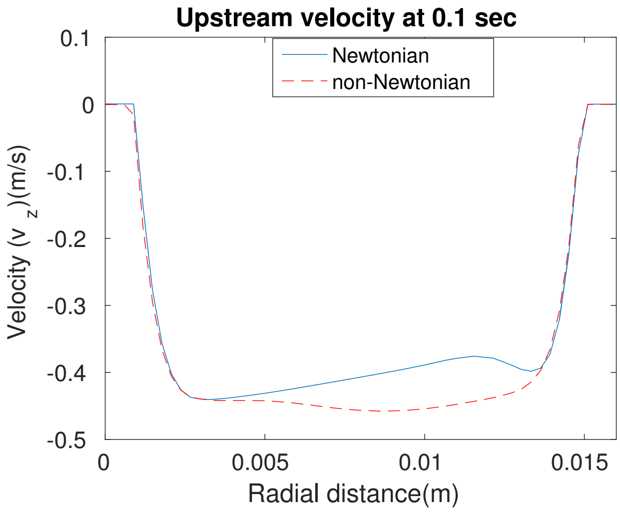

(a) Upstream velocity at 0.1 sec

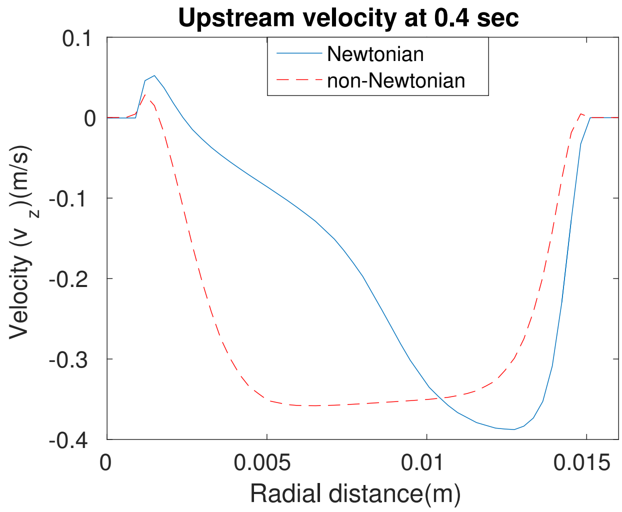

(b) Upstream velocity at 0.4 sec

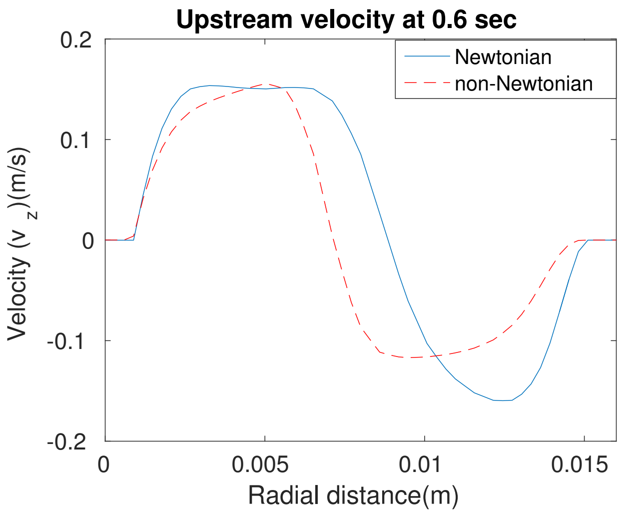

(c) Upstream velocity at 0.6 sec

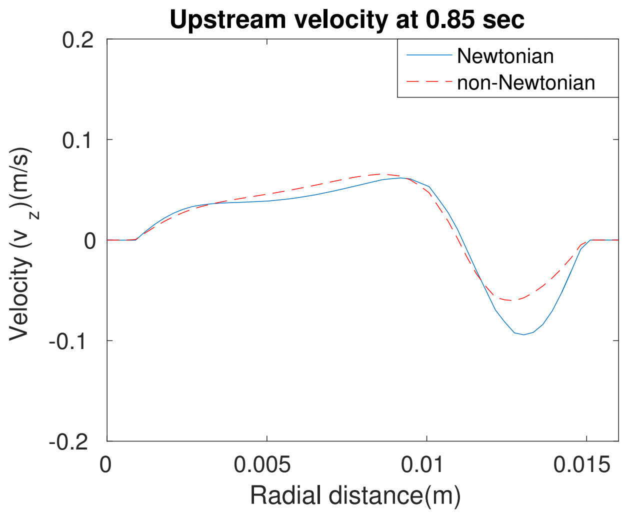

(d) Upstream velocity at 0.85 sec

Figure 4.10: Velocity profiles of Newtonian and non-Newtonian blood at the entrance for 60 BPM 145/80 mm.Hg

4.3.2 Peak deceleration at (t)=0.4 s

At $t = 0.4$ seconds, peak deceleration occurs which means that R_e decreases rapidly. We notice a distinct flow separation that occurs in the mid portion of the stent graft but the onset of which begins at the entrance seen on figure 4.15. This flow separation occurs because of complex secondary flow structures that are developed due to curvature effects. At the onset of curvature, lateral centripetal acceleration occurs which causes a pressure gradient in the radial direction. This ensures that the faster moving fluid is swept outwards and the slower moving fluid is pushed towards the vessel wall. As seen in plot 4.10b, at the entrance non-Newtonian profile varies significantly compared to the Newtonian profile. This is an indication of larger separation region, whereas at the exit, as the curvature effect completely reduces,

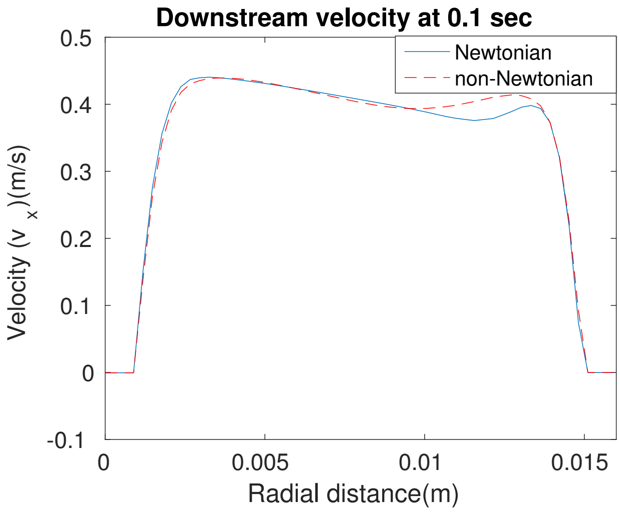

(a) Upstream velocity at 0.1 sec

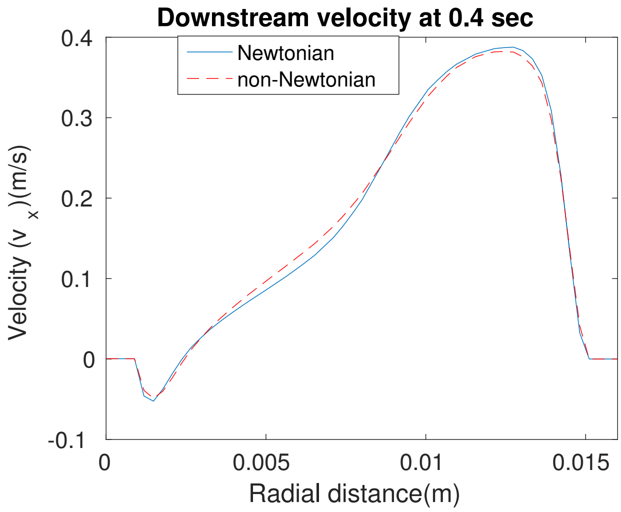

(b) Upstream velocity at 0.4 sec

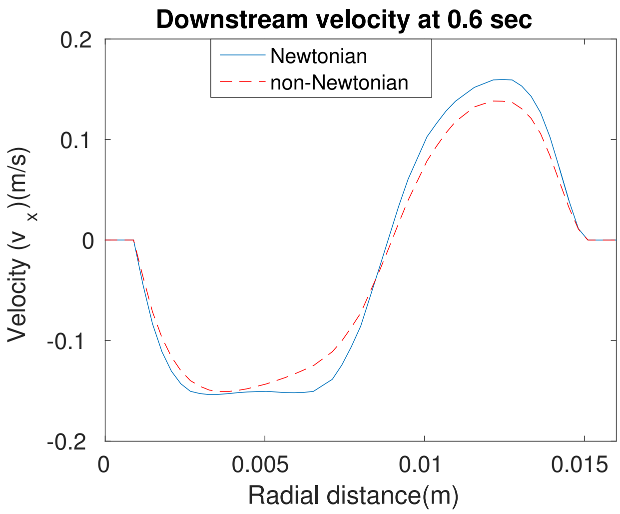

(c) Upstream velocity at 0.6 sec

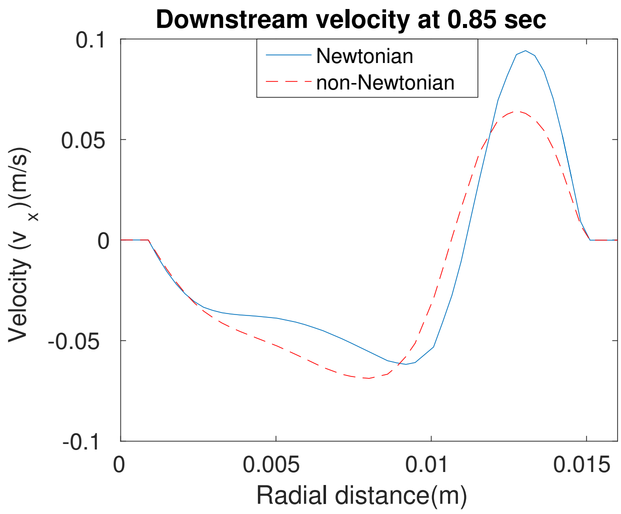

(d) Upstream velocity at 0.85 sec

Figure 4.11: Velocity profiles of Newtonian and non-Newtonian blood at the exit for 60 BPM 145/80 mm.Hg

the profiles are similar as evidenced in figure 4.11b.Velocity gradients remain similar at this stage with small variations the mid region as seen in figures 4.12b and 4.12f in the upstream region.

4.3.3 End of deceleration at (t)=0.6 s

At $t = 0.6$ seconds, the diastolic cycle begins. This is where the R_e tends to zero and viscous effects take precedence. Secondary flow structures are enhanced and recirculation occurs as seen in figure4.16.However, velocities close to the outer wall try to attain a similar velocity as the inner wall as evidenced in figures 4.12c, 4.12g. The non-Newtonian velocity magnitude as expected significantly reduces as there is better viscosity prediction near the wall. Vortex formation is heavily dependent

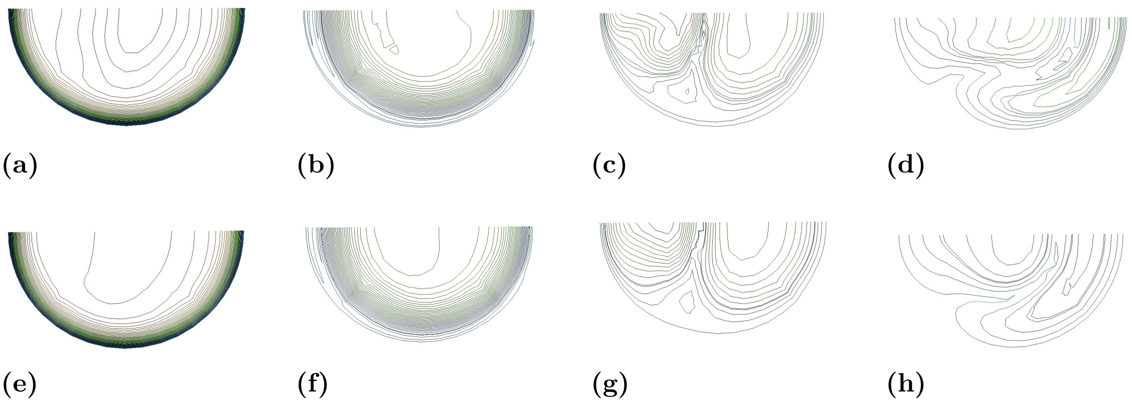

Figure 4.12: Velocity contours of (a)-(d)Newtonian and (e)-(h)non-Newtonian blood at time(t)=0.1, 0.4, 0.6 and 0.85 seconds the entrance for 60 BPM 145/80 mm.Hg

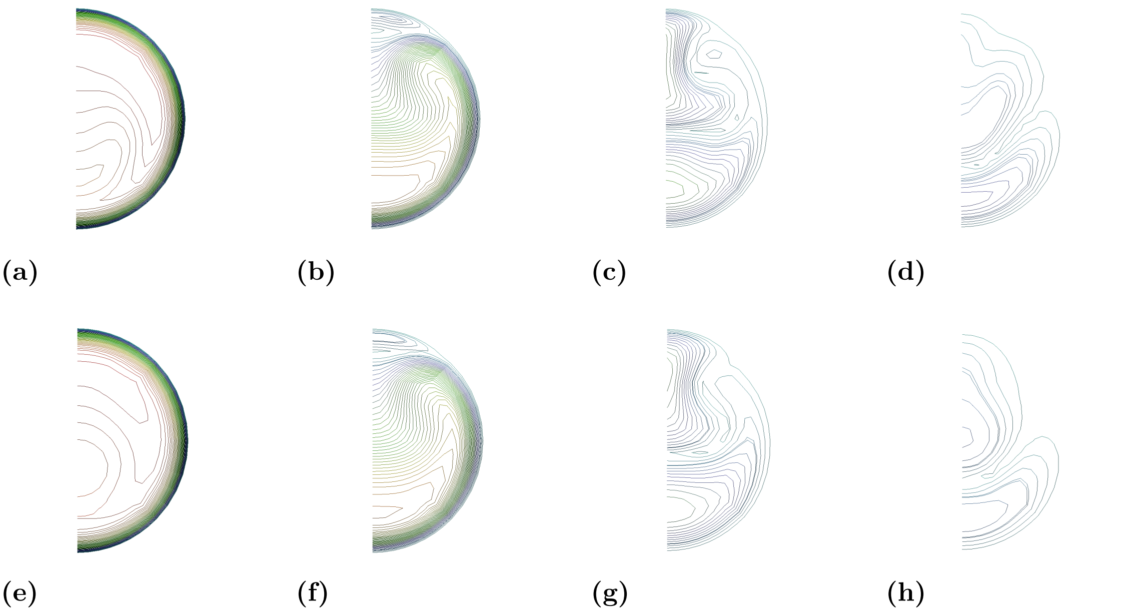

Figure 4.13: Velocity contours of (a)-(d)Newtonian and (e)-(h)non-Newtonian blood at time(t)=0.1, 0.4, 0.6 and 0.85 seconds the exit for 60 BPM 145/80 mm.Hg

on adverse pressure gradient created and friction at the wall and this tends to be lower in non-Newtonian models [7]. Positive to negative variation in the velocities as seen in plots 4.10c and 4.11c are because of the flow separation region. Velocity magnitude is greater at the inner wall, but a far greater outer velocity magnitude is seen in plot 4.10c for Newtonian model.

4.3.4 End of diastole at (t)=0.85 s

At $t = 0.85$ seconds, the diastolic almost ends. This is where the R_e is constant . An accurate prediction of the flow structures in this region is difficult as the flow

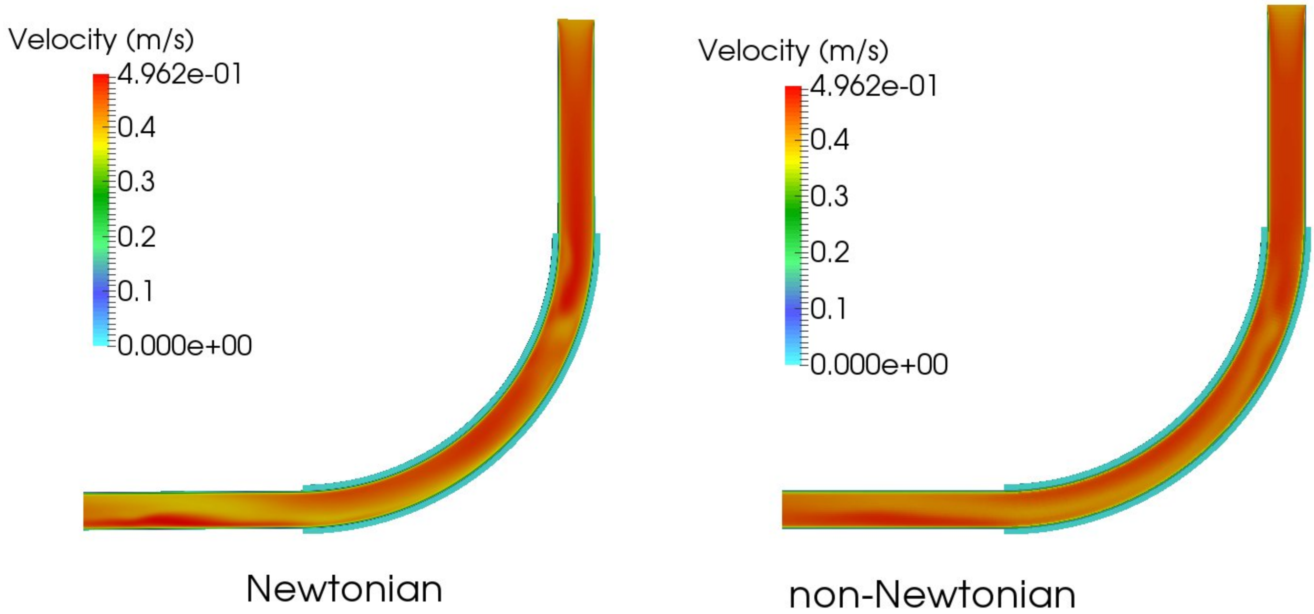

(a) **(b)**

Figure 4.14: Velocity contours for (a)Newtonian and (b)non-Newtonian 60 BPM 145/80 mm.Hg at 0.1 seconds

becomes very chaotic. However, as seen in figure4.17, a vortex structure is formed at the entrance region due to reduction in D_e. This could be the low velocity counter rotating vortex called as Dean vortices. Flow separation still occurs at the mid section owing to the curvature effects but the magnitude of velocity decreases that leads to recirculation effects at the exit. The magnitude of non-Newtonian lower is higher compared to Newtonian velocity. Flow separation region decreases further as evidenced in plots 4.10d and 4.11d. Velocity gradients differ significantly between Newtonian and non-Newtonian seen in figures 4.12d, 4.12h and 4.13d, 4.13h.

4.3.5 Wall shear stress (WSS)

WSS is not expected to vary drastically and is expected to have a small magnitude as the viscous contributions are small. By definition, WSS is the gradient of the tangential component of velocity magnitude. Since the axial component dominates the flow in this particular case, the WSS magnitude is small. We see in 4.18 that there is no difference in WSS at 0.1 seconds as the tangential component is negligible. At t=0.45 s, we see a slight variation of WSS in figure 4.19. Further variation at the entrance and significantly at the exit can be witnessed in figure4.20. We observe a smoother variation for WSS in 4.21the non-Newtonian profile as there is a better prediction of viscosity near the wall , hence the tangential component increases.

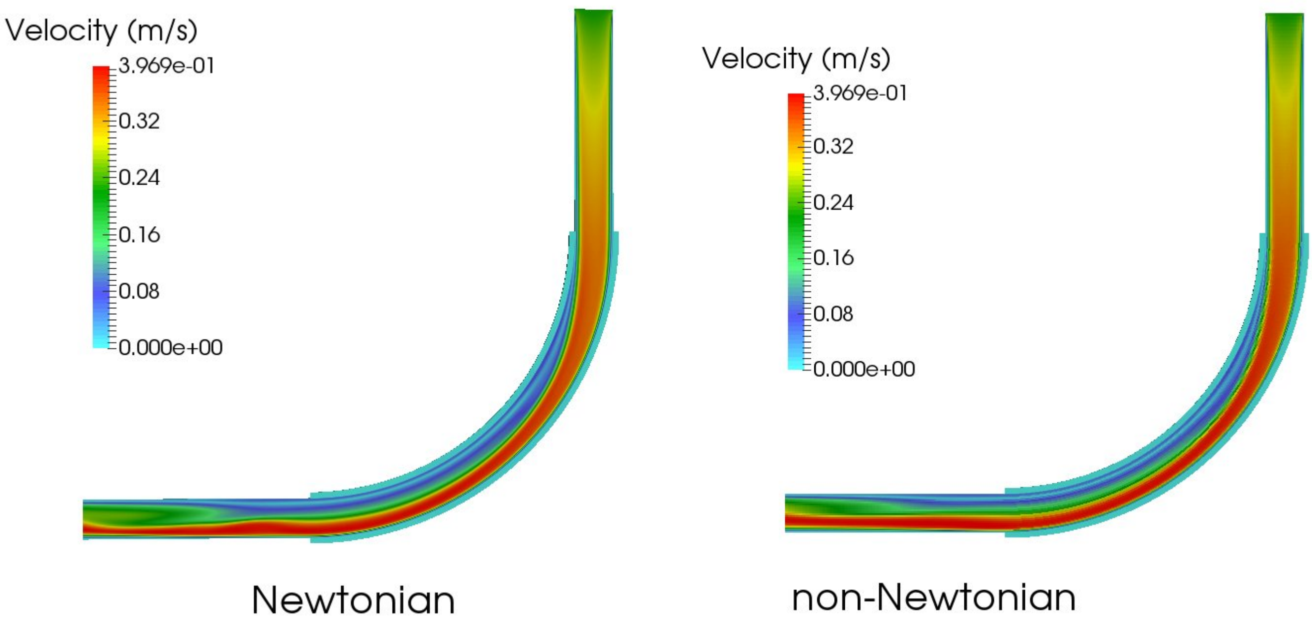

(a) **(b)**

Figure 4.15: Velocity contours for (a)Newtonian and (b)non-Newtonian 60 BPM 145/80 mm.Hg at 0.4

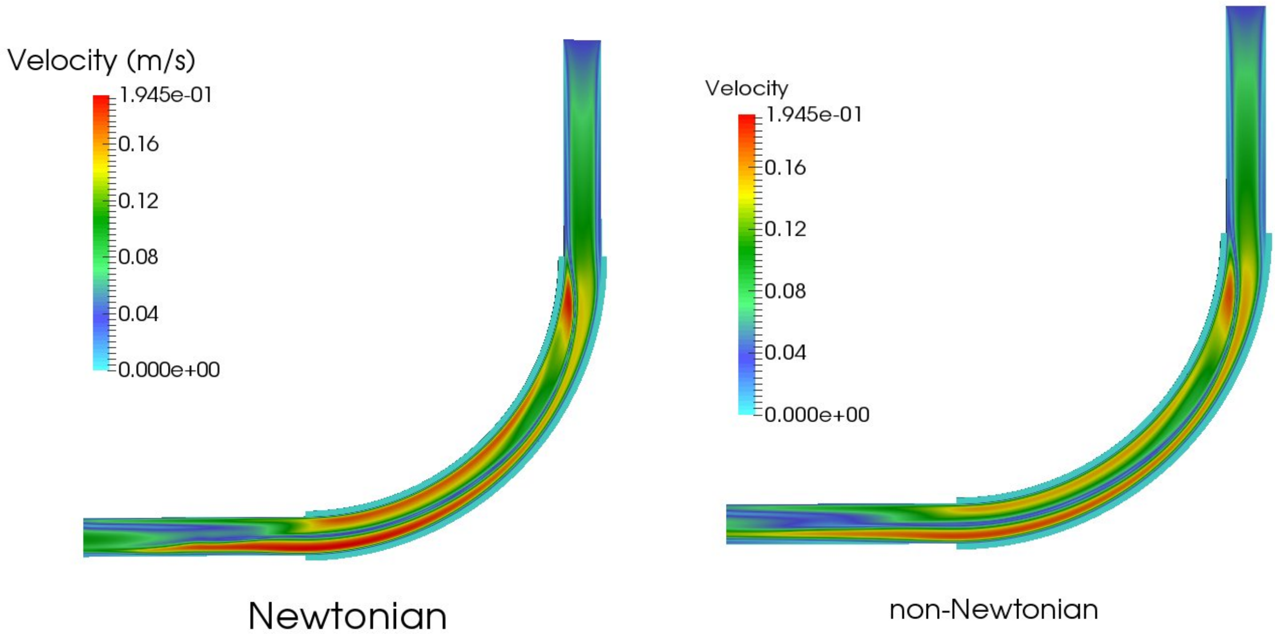

(a) **(b)**

Figure 4.16: Velocity contours for (a)Newtonian and (b)non-Newtonian 60 BPM 145/80 mm.Hg at 0.6

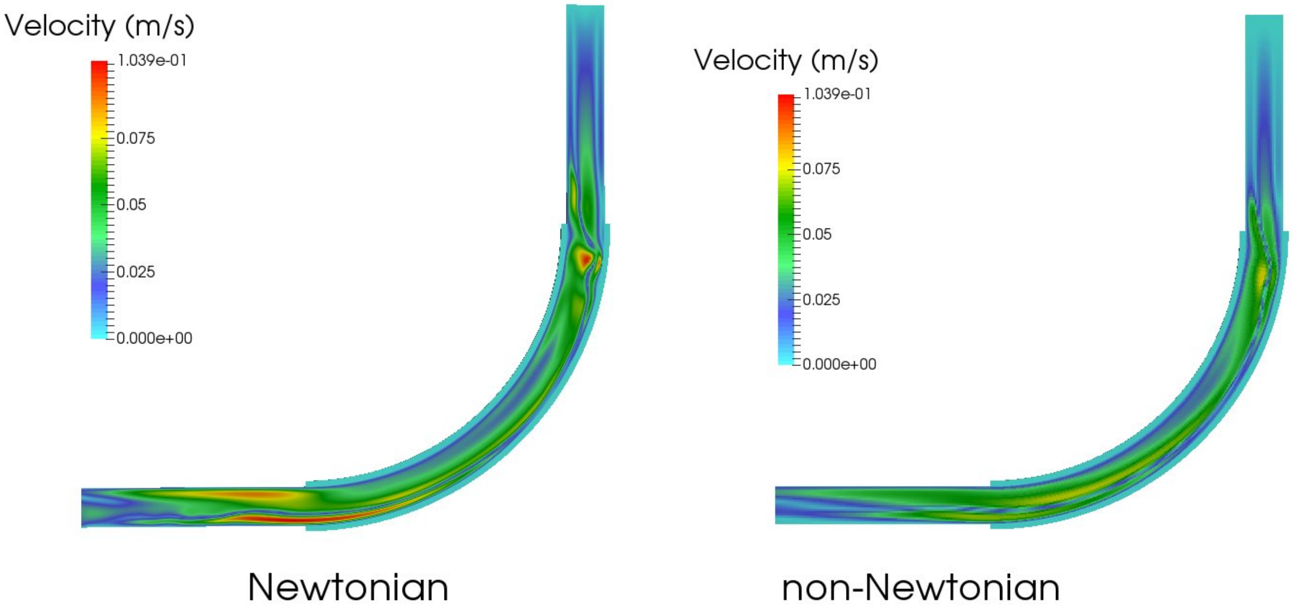

(a) **(b)**

Figure 4.17: Velocity contours for (a)Newtonian and (b)non-Newtonian 60 BPM 145/80 mm.Hg at 0.85

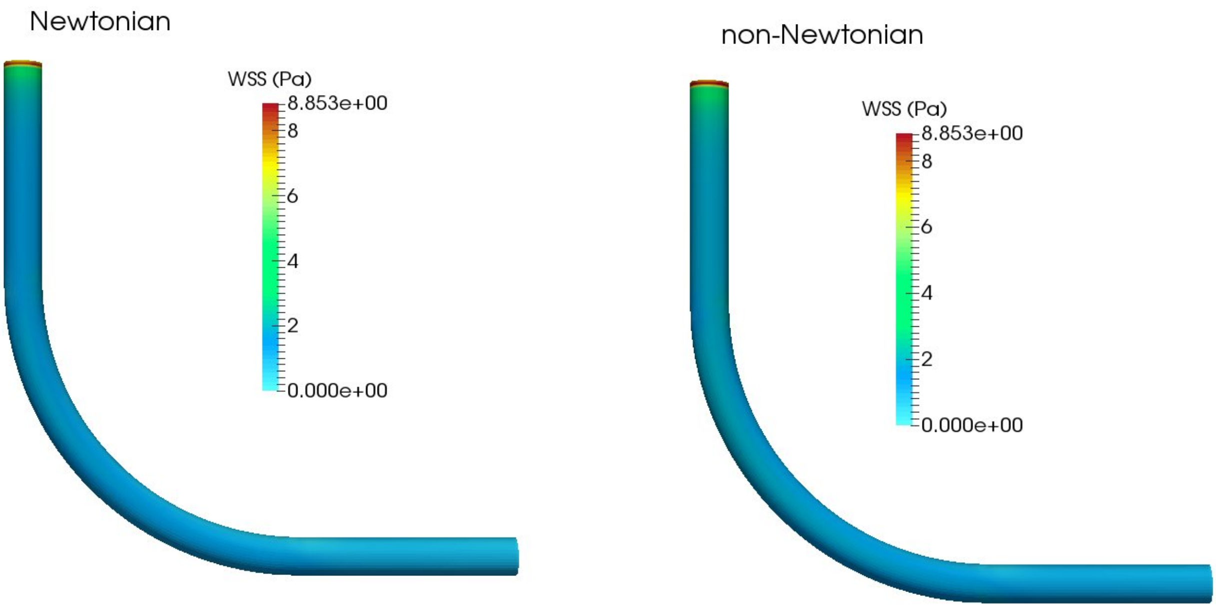

(a) **(b)**

Figure 4.18: WSS for (a)Newtonian and (b)non-Newtonian 60 BPM 145/80 mm.Hg at 0.1s

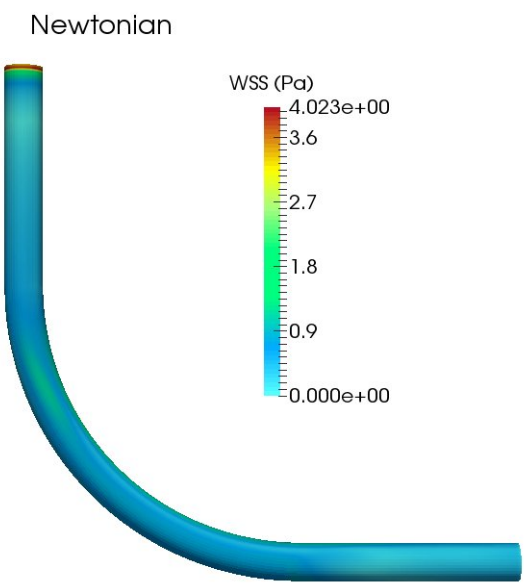

(a)

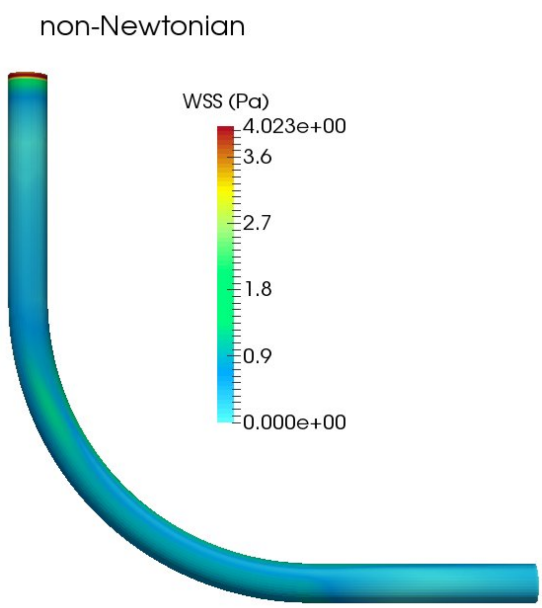

(b)

Figure 4.19: WSS for (a)Newtonian and (b)non-Newtonian 60 BPM 145/80 mm.Hg at 0.4s

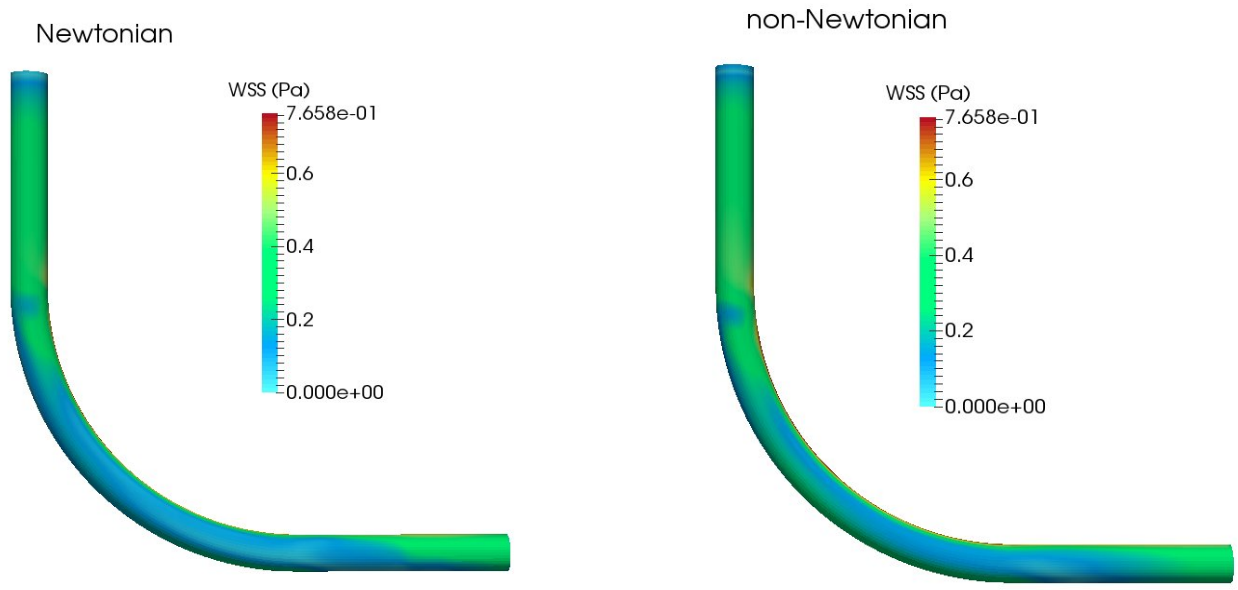

(a) **(b)**

Figure 4.20: WSS for (a)Newtonian and (b)non-Newtonian 60 BPM 145/80 mm.Hg at 0.6s

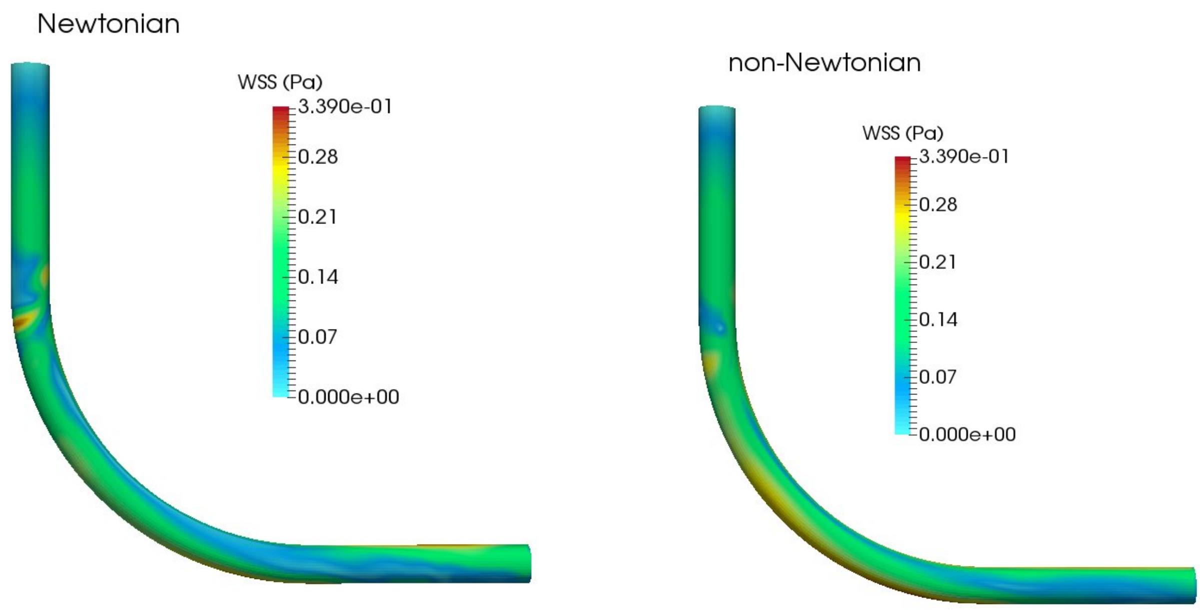

(a) **(b)**

Figure 4.21: WSS for (a)Newtonian and (b)non-Newtonian 60 BPM 145/80 mm.Hg at 0.85s

5
Conclusion and Future Work

5.1 Observations and Conclusions

One of the main objectives of the masters thesis was to compare the experimental results obtained by Roos et al[16] with the developed computational model using water as the fluid medium. We observe that forces obtained in the computational model did not match the experiment except for a pressure of 195/100 mmHg. The gradient of difference between the forces obtained are however similar. The sideways displacement force at the mid portion of the stent graft obtained for 195/100 mm.Hg is similar to the value obtained by Roos et al and Li Kleinstreuer.[16, 11]. Subsequently, after using blood as the fluid medium, no changes were observed in the displacement forces. Temporal variation of drag forces are similar to the exit pressure waveform used for both blood and water.
Another scope was to indicate the importance of pressure and viscous forces. As seen from 4.2.2, pressure is the main cause for displacement forces and the viscous force contribution is insignificant. This could be a compelling argument for using water in the experiments by Roos et al[16].
Evaluating non-Newtonian behaviour and comparing the same with Newtonian blood model is another scope of the project. There were no observable changes between Newtonian and non-Newtonian magnitudes of displacement forces. Viscous force differences were also negligible between the two which further shows viscosity plays a minimal role in the outcome evaluating forces.
Complex secondary flow structures are formed during deceleration phase of the cardiac cycle. Flow separation is attributed to local curvature effects and increasing Dean number(D_e) which causes a radial pressure gradient. At the diastolic phase, the non-Newtonian effects are further visible with reduced velocity magnitudes compared to Newtonian model. Vortices are weakened in the non-Newtonian model due to difference between friction at the wall and pressure gradient [7]. Negligible differences in WSS as observed between Newtonian and non-Newtonian model.

5.2 Future Work

Geometrically: A parametric study similar to [18] could be carried out where diameter changes and different angulations are studied to see the geometric effects on temporal variation of displacement forces.
Structurally: Graft material is assumed to be linear isotropic when in reality the material. It would be interesting to study the non-linear and orthotropic nature of

the material.
Fluid: This is the area which is wide open for future work. Accurate turbulence models can be used to study the evolution of flow structures developed. A 3-D model could be used to study vortex structures in detail.
Other: A 1-D simulink model to map dynamic variations of pressure and velocity. This is to develop an accurate computational model similar to the experimental conditions.

Bibliography

[1] C Alberto Figueroa et al. "Effect of Curvature on Displacement Forces Acting on Aortic Endografts: A 3-Dimensional Computational Analysis". In: *J Endovasc Ther* 16 (2009), pp. 284–294. ISSN: 1526-6028. DOI: 10.1583/08-2667.1.

[2] Patrik Andersson and Johan Pilqvist. "Fluid-Structure Interaction analysis of the forces causing stent graft migration". PhD thesis. 2011, p. 48.

[3] Jacopo Biasetti, Fazle Hussain, and T Christian Gasser. "Blood flow and coherent vortices in the normal and aneurysmatic aortas: a fluid dynamical approach to intra-luminal thrombus formation". In: *Journal of The Royal Society Interface* 8.63 (2011), pp. 1449–1461. ISSN: 1742-5689. DOI: 10.1098/rsif.2011.0041.

[4] Young I Cho and Kenneth R Kensey. "Effects of the non-Newtonian viscosity of blood on flows in a diseased arterial vessel. Part 1: Steady flows." In: *Biorheology* 28.3-4 (1991), pp. 241–262. ISSN: 0006355X.

[5] Efstratios Georgakarakos et al. "Modeling and computational analysis of the hemodynamic effects of crossing the limbs in an aortic endograft ("ballerina" position)." In: *Journal of endovascular therapy : an official journal of the International Society of Endovascular Specialists* 19.4 (2012), pp. 549–57. ISSN: 1545-1550. DOI: 10.1583/12-3820.1.

[6] Carine Guivier-Curien et al. "Analysis of blood flow behaviour in custom stent grafts". In: *Journal of Biomechanics* 42.11 (2009), pp. 1754–1761. ISSN: 00219290. DOI: 10.1016/j.jbiomech.2009.03.053.

[7] Takuji Ishikawa, Shuzo Oshima, and Ryuichiro Yamane. "Vortex enhancement in blood flow through stenosed and locally expanded tubes". In: *Fluid Dynamics Research* 26.1 (2000), pp. 35–52. ISSN: 01695983. DOI: 10.1016/S0169-5983(98)00047-1.

[8] Jo Janela, Alexandra Moura, and Ad??lia Sequeira. "A 3D non-Newtonian fluid-structure interaction model for blood flow in arteries". In: *Journal of Computational and Applied Mathematics* 234.9 (2010), pp. 2783–2791. ISSN: 03770427. DOI: 10.1016/j.cam.2010.01.032.

[9] Barbara M Johnston et al. "Non-Newtonian blood flow in human right coronary arteries: Steady state simulations". In: *Journal of Biomechanics* 37.5 (2004), pp. 709–720. ISSN: 00219290. DOI: 10.1016/j.jbiomech.2003.09.016.

[10] Safoora Karimi et al. "Effect of rheological models on the hemodynamics within human aorta: CFD study on CT image-based geometry". In: *Journal of*

Non-Newtonian Fluid Mechanics 207.April (2014), pp. 42–52. ISSN: 03770257. DOI: 10.1016/j.jnnfm.2014.03.007.

[11] Z. Li and C. Kleinstreuer. “Analysis of biomechanical factors affecting stent-graft migration in an abdominal aortic aneurysm model”. In: *Journal of Biomechanics* 39.12 (2006), pp. 2264–2273. ISSN: 00219290. DOI: 10.1016/j.jbiomech.2005.07.010.

[12] Z. Li and C. Kleinstreuer. “Fluid-Structure Interaction Effects on Sac-Blood Pressure and Wall Stress in a Stented Aneurysm”. In: *Journal of Biomechanical Engineering* 127.4 (2005), pp. 662–671. ISSN: 01480731. DOI: 10.1115/1.1934040.

[13] Zhonghua Li and Clement Kleinstreuer. “Blood flow and structure interactions in a stented abdominal aortic aneurysm model”. In: *Medical Engineering and Physics* 27.5 (2005), pp. 369–382. ISSN: 13504533. DOI: 10.1016/j.medengphy.2004.12.003.

[14] K Liffman et al. “Analytical modeling and numerical simulation of forces in an endoluminal graft.” In: *Journal of endovascular therapy : an official journal of the International Society of Endovascular Specialists* 8.4 (2001), pp. 358–71. ISSN: 1526-6028. DOI: 10.1583/1545-1550(2001)008<0358:AMANSO>2.0.CO;2.

[15] Prashanta Kumar Mandal. “An unsteady analysis of non-Newtonian blood flow through tapered arteries with a stenosis”. In: *International Journal of Non-Linear Mechanics* 40.1 (2005), pp. 151–164. ISSN: 00207462. DOI: 10.1016/j.ijnonlinmec.2004.07.007.

[16] H. Roos et al. “Displacement forces in iliac landing zones and Stent graft interconnections in endovascular aortic repair: An experimental study”. In: *European Journal of Vascular and Endovascular Surgery* 47.3 (2014), pp. 262–267. ISSN: 10785884. DOI: 10.1016/j.ejvs.2013.11.015.

[17] R Skalak, S R Keller, and T W Secomb. “Mechanics of blood flow.” In: *Journal of biomechanical engineering* 103.May 1981 (1981), pp. 102–115. ISSN: 0148-0731.

[18] Mikhail Tokarev et al. “DIC for Surface Motion Analysis Applied to Displacement of a Stent Graft for Abdominal Aortic Repair in a Pulsating Flow”. In: ().

[19] Zeljko Tukovic and Hrvoje Jasak. “Updated Lagrangian finite volume solver for large deformation dynamic response of elastic body”. In: *Transactions of Famena* 31.1 (2007), pp. 55–70. ISSN: 13331124.

[20] Jiyuan Tu; Kiao Inthavong; Kelvin Kian Loong Wong. *Computational Hemodynamis-Theory, Modelling and Applications*. Vol. 53. 9. 2015, pp. 21–35. ISBN: 9788578110796. DOI: 10.1017/CBO9781107415324.004. arXiv: arXiv:1011.1669v3.

[21] Fuat Yilmaz and Mehmet Yasar Gundogdu. “A critical review on blood flow in large arteries; relevance to blood rheology, viscoisty models and physiologic conditions”. In: *Kore-Australia Rheology Journal* 20.4 (2008), pp. 197–211. ISSN: 1226119X.